Fock-Darwin states of anisotropic quantum dots with Rashba spin-orbit coupling

by

Siranush Avetisyan

A Thesis submitted to the Faculty of Graduate Studies of

The University of Manitoba

in partial fulfilment of the requirements of the degree of

MASTER OF SCIENCE

Department of Physics and Astronomy

University of Manitoba

Winnipeg

Abstract

Here I report on our studies of the electronic properties of elliptical quantum dots in a perpendicular external magnetic field, and in the presence of the Rashba spin-orbit interaction. Our work indicates that the Fock-Darwin spectra, corresponding to the non-interacting electrons in an elliptical quantum dot display a strong signature of the Rashba spin-orbit coupling even in a low magnetic field, as the anisotropy of the quantum dot is increased. An explanation of this pronounced effect with respect to the anisotropy is presented. The strong spin-orbit coupling effect manifests itself prominently in the corresponding dipole-allowed optical transitions and hence is susceptible to direct experimental observation.

Acknowledgments

The theoretical work presented in this thesis was carried out at the University of Manitoba under the supervision of Professor Tapash Chakraborty. I would like to thank him for providing me the opportunity to study in Canada and for suggesting me to work on such an important and interesting topic. I also thank him for his help in scientific matters, for his support during all my studies and for the interesting discussions that we had throughout the course of the work. I would like also to mention Dr. Pekka Pietiläinen from the University of Oulu, Finland for his help throughout. We have been in touch remotely and he has been always ready with important and crucial advice about the computational aspects of the work and other related issues in general. I thank him for his support and patience.

Contents

6 Appendices

List of Figures

List of Abbreviations

QD quantum dot

SO spin-orbit

SOI spin-orbit interaction

List of Symbols

m^* electron effective mass

m_0 free electron mass

c speed of light

θ angular coordinate

r radial coordinate

ψ one-electron eigenfunction

ω_0 confinement potential strength

ω_c cyclotron frequency

n principal angular momentum

ℓ orbital angular momentum

g Lande factor

μ_B Bohr magneton

α Rashba SOI constant

β Dresselhaus SOI constant

$\boldsymbol{\sigma}$ Pauli matrices

$\hat{\varepsilon}$ polarization

γ polarization angle w.r.t unrotated x axis

α_F fine structure constant

Publications

Physical Review B **85**, 153301 (2012)

Siranush Avetisyan, Pekka Pietiläinen, Tapash Chakraborty

Strong enhancement of Rashba spin-orbit coupling with increasing anisotropy in the Fock-Darwin states of a quantum dot

Physical Review B **86**, 239901(E) (2012)

Siranush Avetisyan, Pekka Pietiläinen, Tapash Chakraborty

Erratum: Strong enhancement of Rashba spin-orbit coupling with increasing anisotropy in the Fock-Darwin states of a quantum dot

[Phys. Rev. B 85, 153301 (2012)]

1 Introduction

Quantum dots are one of the most interesting systems in semiconductor nanostructures and have been studied extensively for more than two decades. Besides being an interesting physical system where a host of novel physical phenomena have been explored, a quantum dot is also interesting from the technological point of view, in particular, for lasers, quantum cryptography, and quantum computations, just to name a few. A quantum dot (QD) [1,2] is a nanometer size planar system consisting of a few electrons. It shows very strong quantum mechanical properties due to its nanoscale size. A QD is in fact a quasi-zero-dimensional electron system where the motion of electrons is confined in all three spatial dimensions leading to a discrete energy spectrum. This discrete energy spectrum and the man-made confining potential characterize a quantum dot as an *artificial atom* [1]. The usual energy level spacing of a quantum dot lies in the range of a few meV. These characteristics provide a unique opportunity to study the atomic-like properties of the QDs. Unlike in a real atom, here the confinement potential and the number of electrons can be controlled externally. Due to the larger size of the QDs compared to the actual atoms, these artificial atoms are suitable for many experiments [3,4] that are almost impossible to carry out in atomic systems.

Another important direction of the QD research that is gaining popularity recently is the role of the spin-orbit interactions (SOI) in quantum dots. The spin-orbit (SO) interactions [5] arise in quantum dots by various mechanisms related to the electron confinement and the symmetry breaking and are generally introduced in the Hamiltonian via the Rashba [6,7] and the Dresselhaus [8] form of the interaction. The Rashba interaction stems from the structural inversion asymmetry as introduced by a heterojunction or by the external fields. In

semiconductors with a narrow energy gap, this effect is expected to be strong. The Dresselhaus interaction, on the other hand, originates from the bulk inversion asymmetry of the crystal and can be relatively large in semiconductors such as InSb/InAlSb. It has been experimentally shown that the Rashba spin-orbit interaction can be modified up to 50% by an external gate voltage. This interesting possibility of *tuning* the spin-orbit field and thereby coherently manipulating the electron spins in quantum dots has sparked major activities in recent years. In our present work, we focus entirely on the Rashba SO interaction [9]. The SO coupling in nanostructured systems, such as the semiconductor QDs, is highly interesting because of its relevance to spin transport in low-dimensional electron channels. The form of the Rashba spin-orbit interaction is described by the Hamiltonian $H_{SO} = \frac{\alpha}{\hbar}\left[\boldsymbol{\sigma} \times \left(\mathbf{p} - \frac{e}{c}\mathbf{A}\right)\right]_z$, where the electron charge is $e = -|e|$, α is the spin-orbit coupling constant, which is sample dependent and is proportional to the interface electric field that confines the electrons in the xy plane, $\boldsymbol{\sigma} = \left(\sigma_x, \sigma_y, \sigma_z\right)$ denotes the Pauli matrices, $\mathbf{p} = \left(p_x, p_y, p_z\right)$ corresponds to the particle momentum and $\mathbf{A}$ is the vector potential. The Dresselhaus spin-orbit interaction is usually expressed as $H_{SO}^{D} = \frac{\beta}{\hbar}\left(\sigma_x p_x - \sigma_y p_y\right)$, where β is the coupling parameter. The other spin dependent interaction is the Zeeman interaction which arises from a direct coupling with an applied magnetic field of the intrinsic magnetic moment associated with the electron spin.

For more than two decades, theoretical studies of QDs in an external magnetic field have largely focused on the properties of quantum dots with circular symmetry [1,2]. Extensive investigations of transport and optical spectroscopy of these semiconductor nanostructures have revealed

several important atomic-like properties [1,2]. It has been found that the SO coupling for circularly symmetric QDs mainly causes multiple level crossings and level repulsion [10] in the energy spectra, however, the level repulsions were very weak [11] in those systems.

In contrast to QDs with circular symmetry, not enough is known about the electronic properties of anisotropic quantum dots, although a few theoretical and experimental papers have been already available in the literature [12,13]. For example, no studies of the Rashba effect in an elliptical QD have been reported as yet. In the present work [14], we have focused on the electronic properties of elliptical quantum dots in a perpendicular external magnetic field, and in the presence of the Rashba spin-orbit coupling. As mentioned above, the electronic properties of elliptical QDs in a strong magnetic field without the SOI have already been studied earlier both theoretically and experimentally almost two decades ago [12,13], when it was found that the major effect of anisotropy was to lift the degeneracies of the single-particle energy spectrum [12,13]. In our work [14] we have shown that the Fock-Darwin spectra [1,2] display a major enhancement of the Rashba spin-orbit coupling even in a low magnetic field, when the anisotropy of the quantum dot is increased. This prominent effect of the SOI predicted in our work is expected to be confirmed experimentally [1,2], which would provide an useful step forward to control the SO coupling in nanostructures, en route to semiconductor spintronics [15].

2 The Hamiltonian

As stated above, the quantum dots are nanoscale structures in which electrons are confined by a lateral potential that is applied in the plane of a two-dimensional electron system [1,2]. The electrons are confined electrostatically at the semiconductor interface by various arrangements of metallic gates. The shape and magnitude of the confinement potentials of electrons are controlled via the voltages applied to each of those metallic gates. The most popular choice of the confinement potential has been a parabolic potential [1] in the electron plane. This model of a QD has been demonstrated, theoretically as well as experimentally, to contain all essential physics of the dots. The quantum states of two-dimensional circular dots are characterized by the rotational symmetry that gives rise to level degeneracy at the zero field.

The problem of finding the wave functions and the energy eigenvalues of an electron in a magnetic field was discussed by Landau in 1930 [16]. Following his work, the Hamiltonian of a single electron is written as

$$H = \frac{1}{2m^*}\left(\boldsymbol{p} - \frac{e}{c}\boldsymbol{A} \right)^2 \tag{2.1}$$

where m^* is the effective mass of the electron. If we choose the symmetric gauge vector potential $\mathbf{A} = \frac{1}{2}B(-y, x, 0)$ and $e = -|e|$, then the Schrodinger equation is written as

$$\frac{-\hbar^2}{2m^*}\left\{ \frac{\partial^2\psi}{\partial r^2} + \frac{1}{r}\frac{\partial\psi}{\partial r} + \frac{1}{r^2}\frac{\partial^2\psi}{\partial\theta^2} \right\} - \frac{ieB\hbar}{2m^*c^2}\frac{\partial\psi}{\partial\theta} + \left(\frac{e^2B^2r^2}{8m^*c^2} - E \right)\psi = 0. \tag{2.2}$$

Let, $\psi = \frac{1}{\sqrt{2\pi}} f(r) e^{-i\ell\theta}$. The radial part of the equation (2.2) is then

$$\frac{-\hbar^2}{2m^*}\left(\frac{d^2f}{dr^2} + \frac{1}{r}\frac{df}{dr} - \frac{\ell^2}{r^2} f \right) - \frac{eB\hbar}{2m^*c}\ell f + \left(\frac{e^2B^2r^2}{8m^*c^2} - E \right) f = 0. \tag{2.3}$$

Defining the cyclotron frequency $\omega_c = \frac{eB}{m^* c} = \frac{\hbar}{m^* \ell_0^2}$, and the magnetic length $\ell_0 \equiv \left(\frac{\hbar c}{eB}\right)^{1/2}$, the radial equation is simplified to

$$\frac{\hbar^2}{2m^*}\left(f'' + \frac{f'}{r} - \frac{\ell^2}{r^2} f \right) + \left(E - \frac{1}{8} m^* \omega_c^2 r^2 + \frac{1}{2} \hbar \omega_c \ell \right) f = 0. \tag{2.4}$$

Let us define a new independent variable $x = \frac{m^* \omega_c}{2\hbar} r^2 = a r^2 = \frac{r^2}{2\ell_0^2}$. Then the radial equation (2.4) transforms into

$$x f'' + f' - \frac{\ell^2 f}{4x} + \left(\frac{E}{\hbar \omega_c} - \frac{1}{4} x + \frac{1}{2} \ell \right) f = 0 . \tag{2.5}$$

The further simplification of the radial equation follows if we define $\eta = E / \hbar \omega_c + \ell / 2$,

$$x f'' + f' + \left(\eta - \frac{1}{4} x - \frac{\ell^2}{4x} \right) f = 0 . \tag{2.6}$$

The single-electron eigen-energies (Landau levels) are then obtained from the solution of equation (2.6)

$$\begin{aligned} E_{n,\ell} &= \frac{1}{2} \hbar \omega_c \left(2n + |\ell| + 1 - \ell \right) \\ &= \left(2n + |\ell| + 1 \right) \hbar \tilde{\Omega} - \frac{1}{2} \hbar \ell \omega_c , \end{aligned} \tag{2.7}$$

where $\tilde{\Omega} = \omega_c / 2$. Here the two quantum numbers are $n = 0, 1, 2, ...$ the radial quantum number and $\ell = 0, \pm 1, \pm 2, ...,$ the azimuthal quantum number.

The problem of a single electron in a circular (planar) dot confined by a parabolic potential in the presence of an external magnetic field was solved more than a half century ago by Fock (1928) and later by Darwin (1930) [1]. The Hamiltonian of such a system is given by

$$H = \frac{1}{2m^*} \left(\boldsymbol{p} - \frac{e}{c} \boldsymbol{A} \right)^2 + V_{\text{conf}}\left(x, y \right), \tag{2.8}$$

where $V_{\text{conf}} = \frac{1}{2} m^* \omega_0^2 \left(x^2 + y^2 \right)$ is the confinement potential. The derivation of the eigen-energies is similar to the case outlined above, but with the confinement potential included

$$E_{n_1,n_2} = \left(n_1 + 1 \right) \hbar\Omega + \frac{1}{2} \hbar\omega_c n_2 , \tag{2.9}$$

where Ω is now expressed as $\Omega^2 = \omega_0^2 + \frac{\omega_c^2}{4}$. The quantum numbers are $n_{1,2} = n_x \pm n_y$ for $n_x, n_y = 0,1,...$ The quantum numbers $n_{1,2}$ can in turn be expressed in terms of conventional quantum numbers, the principal quantum number $n = 0,1,2,...$ and orbital angular momentum $\ell = 0, \pm 1, \pm 2, ...,$ as $n_1 \equiv 2n + |\ell|$, $n_2 \equiv -\ell$. The energy spectrum is then given by

$$E_{n,\ell}(B) = \left(2n + |\ell| + 1 \right) \hbar\Omega - \frac{\ell}{2} \hbar\omega_c \tag{2.10}$$

Figure 1.1. Fock-Darwin energy levels of an isotropic quantum dot as a function of the magnetic field B (in Tesla) with external confinement of $\hbar\omega_0 = 4\,\text{meV}$. The levels are indicated by their quantum numbers (n, ℓ).

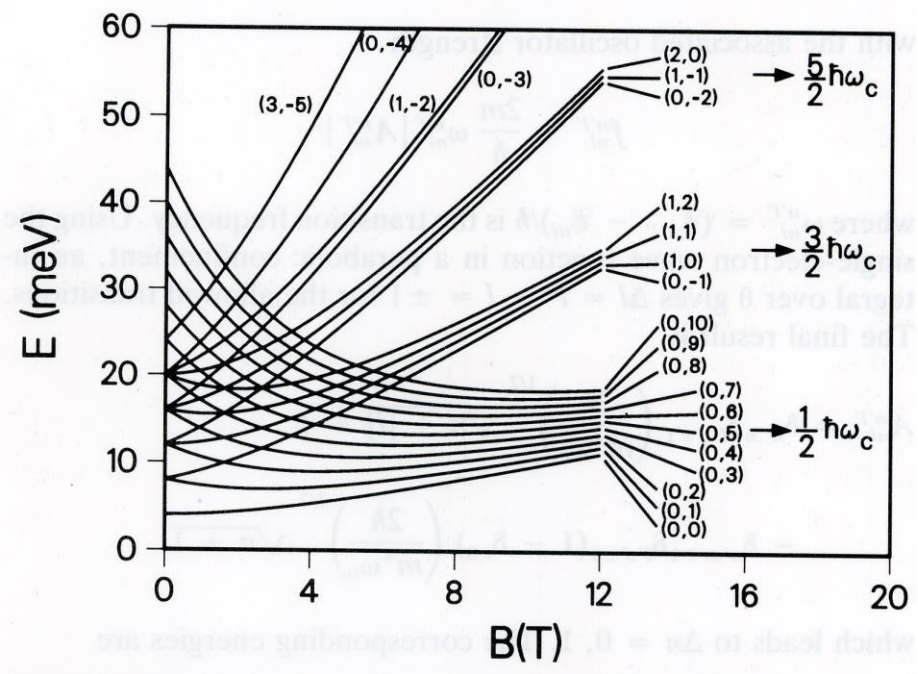

The single-electron QD levels are displayed in Fig. 1, given by the Fock-Darwin description of the energy spectrum $E_{n\ell}(B)$ [1,2]. For $B=0$ we have the regularly spaced spectrum of two-dimensional symmetric harmonic oscillator, where the degeneracy becomes larger with higher energies. In the high-field limit $(B\to\infty)$, the lowest energy levels converge into the Landau levels with the effects of the confinement playing an ever decreasing role, i.e. with the increasing magnetic field, the free-electron behaviour prevails over the confinement.

In what follows, we are going to see how the electron levels shift and split, resulting in many level crossings at low magnetic fields, as we introduce the anisotropy in the dot. In addition, we will also show how the application of a spin-orbit coupling turns some of the level crossings in the energy spectra to anti-crossings at nonzero magnetic fields.

2.1 The Single - electron System

Anisotropic QDs, in particular the elliptical dots have been receiving increasing attention lately, due to their unique properties [12, 13]. Unlike circular QDs, the elliptical QDs have reduced symmetry and it is important to investigate their effects on the Fock-Darwin spectrum.

Consider an electron in an anisotropic parabolic confinement potential in the presence of a quantizing perpendicular magnetic field. The Hamiltonian of such a system is again described by the equation (2.8), however the confinement potential now looks different as a result of the anisotropy of the dot:

$$V_{\text{conf}} = \frac{1}{2} m^* \left(\omega_x^2 x^2 + \omega_y^2 y^2\right). \tag{2.11}$$

We choose the symmetric gauge vector potential $\mathbf{A} = \frac{1}{2} B(-y, x, 0)$ and introduce the rotated coordinates and momenta [12]:

$$
\begin{aligned}
x &= q_1 \cos\chi - \chi_2 p_2 \sin\chi \\
y &= q_2 \cos\chi - \chi_2 p_1 \sin\chi \\
p_x &= p_1 \cos\chi + \chi_1 q_2 \sin\chi \\
p_y &= p_2 \cos\chi + \chi_1 q_1 \sin\chi .
\end{aligned}
\tag{2.12}
$$

where

$$
\chi_1 = -\left[\frac{1}{2}\left(\Omega_1^2 + \Omega_2^2\right)\right]^{1/2}, \quad \chi_2 = \chi_1^{-1},
$$

$$
\tan 2\chi = m^* \omega_c \left[2\left(\Omega_1^2 + \Omega_2^2\right)\right]^{1/2} / \left(\Omega_1^2 - \Omega_2^2\right), \tag{2.13}
$$

$$
\Omega_{1,2}^2 = m^{*2}\left(\omega_{x,y}^2 + \frac{1}{4}\omega_c^2\right), \qquad \omega_c = eB/m^* c.
$$

The relations above are consistent with the commutation relations $\left[p_{i,} q_j\right] = -i\hbar\delta_{ij}$ and $\left[q_i, q_j\right] = \left[p_i, p_j\right] = 0$ if $\chi_1\chi_2 = 1$.

In terms of the rotated operators introduced above, the extended Hamiltonian that is written as

$$
H = \frac{1}{2m^*}\left[p_x^2 + \Omega_1^2 x^2 + p_y^2 + \Omega_2^2 y^2 + m^* \omega_c \left(y p_x - x p_y\right)\right] \tag{2.14}
$$

is diagonal [12],

$$
H = \frac{1}{2m^*}\left(\beta_1^2 p_1^2 + \beta_2^2 p_2^2 + \gamma_1^2 q_1^2 + \gamma_2^2 q_2^2\right), \tag{2.15}
$$

where

$$
\beta_1^2 = \frac{\Omega_1^2 + 3\Omega_2^2 + \Omega_3^2}{2\left(\Omega_1^2 + \Omega_2^2\right)}, \qquad \gamma_1^2 = \frac{1}{4}\left(3\Omega_1^2 + \Omega_2^2 + \Omega_3^2\right) \tag{2.16.1}
$$

$$
\beta_2^2 = \frac{3\Omega_1^2 + \Omega_2^2 - \Omega_3^2}{2\left(\Omega_1^2 + \Omega_2^2\right)}, \qquad \gamma_2^2 = \frac{1}{4}\left(\Omega_1^2 + 3\Omega_2^2 - \Omega_3^2\right) \tag{2.16.2}
$$

$$
\Omega_3^2 = \left[\left(\Omega_1^2 - \Omega_2^2\right)^2 + 2m^{*2}\omega_c^2\left(\Omega_1^2 + \Omega_2^2\right)\right]^{1/2}. \tag{2.16.3}
$$

The detailed algebra can be found in Appendix A.

2.2 The Ladder Operators

We write the Hamiltonian

$$H = \frac{1}{2m^*}\left(\beta_1^2 p_1^2 + \beta_2^2 p_2^2 + \gamma_1^2 q_1^2 + \gamma_2^2 q_2^2\right) \tag{2.17}$$

as a sum

$$H = H_1 + H_2 \tag{2.18}$$

where we have set

$$H_i = \frac{1}{2m^*}\left(\beta_i^2 p_i^2 + \gamma_i^2 q_i^2\right), \qquad i = 1,2 \tag{2.19}$$

The fundamental commutation relations

$$\begin{aligned} \left[p_i, q_j\right] &= -i\hbar\delta_{ij} \\ \left[q_i, q_j\right] &= \left[p_i, p_j\right] = 0 \end{aligned} \tag{2.20}$$

imply that these Hamiltonians commute with each other, i.e.,

$$\left[H_1, H_2\right] = 0 \tag{2.21}$$

and hence describe two independent physical systems.

In order to get more physical insight into the system, we now rewrite the Hamiltonian H_i as

$$\begin{aligned} H_i &= \frac{1}{2m^*}\left(\beta_i^2 p_i^2 + \gamma_i^2 q_i^2\right) = \frac{\beta_i^2}{2m^*} p_i^2 + \frac{\gamma_i^2}{2m^*} q_i^2 \\ &= \frac{1}{2\left(m^*/\beta_i^2\right)} p_i^2 + \frac{1}{2}\frac{m^*}{\beta_i^2}\frac{\beta_i^2}{m^*}\frac{\gamma_i^2}{m^*} q_i^2 \\ &= \frac{1}{2m_i} p_i^2 + \frac{1}{2} m_i \omega_i^2 q_i^2 \end{aligned} \tag{2.22}$$

where we have introduced the new quantities

$$
\begin{aligned}
m_i &= \frac{m^*}{\beta_i^2} \\
\omega_i &= \frac{\beta_i \gamma_i}{m^*}.
\end{aligned}
\tag{2.23}
$$

Since the operators p_i and q_i obey the basic commutation relations of position and momentum operators, the final form of the Hamiltonian

$$
H_i = \frac{1}{2m_i} p_i^2 + \frac{1}{2} m_i \omega_i^2 q_i^2 \tag{2.24}
$$

shows that H_i describes a harmonic oscillator with a (fictitious) mass m_i and angular velocity ω_i. Correspondingly, the total Hamiltonian can be thought to describe two independent one-dimensional oscillators.

Let us now see how we can express our Hamiltonian in terms of the ladder operators defined as

$$
\begin{aligned}
a_i &= \sqrt{\frac{m_i \omega_i}{2\hbar}} \left(q_i + \frac{i}{m_i \omega_i} p_i \right) \\
a_i^\dagger &= \sqrt{\frac{m_i \omega_i}{2\hbar}} \left(q_i - \frac{i}{m_i \omega_i} p_i \right).
\end{aligned}
\tag{2.25}
$$

For that purpose we introduce the number operators $N_i = a_i^\dagger a_i$ and determine an explicit expression for them:

$$
\begin{aligned}
N_i = a_i^\dagger a_i &= \frac{m_i \omega_i}{2\hbar} \left(q_i - \frac{i}{m_i \omega_i} p_i \right) \left(q_i + \frac{i}{m_i \omega_i} p_i \right) \\
&= \frac{m_i \omega_i}{2\hbar} \left(q_i^2 + \frac{i}{m_i \omega_i} q_i p_i - \frac{i}{m_i \omega_i} \left(q_i p_i - i\hbar \right) + \frac{1}{m_i^2 \omega_i^2} p_i^2 \right) \\
&= \frac{m_i \omega_i}{2\hbar} \left(q_i^2 + \frac{1}{m_i^2 \omega_i^2} p_i^2 - \frac{\hbar}{m_i \omega_i} \right) \\
&= \frac{1}{\hbar \omega_i} \left(\frac{p_i^2}{2m_i} + \frac{1}{2} m_i \omega_i^2 q_i^2 \right) - \frac{1}{2} = \frac{1}{\hbar \omega_i} H_i - \frac{1}{2}.
\end{aligned}
\tag{2.26}
$$

For the Hamiltonians we now have new expressions

$$H_i = \hbar\omega_i\left(N_i + \frac{1}{2}\right). \tag{2.27}$$

As Hermitian operators the number operators have a complete set of eigenstates with real eigenvalues, i.e., there is a complete set of states $|n_i\rangle$ satisfying the relations

$$\begin{aligned} N_i|n_i\rangle &= n_i|n_i\rangle \\ \langle n_i|n_i'\rangle &= \delta_{n_i,n_i'} \end{aligned} \tag{2.28}$$

Therefore, the eigenstates $|n_i\rangle$ of the number operator are also eigenstates of the Hamiltonians:

$$H_i|n_i\rangle = \left(n_i + \frac{1}{2}\right)\hbar\omega_i|n_i\rangle\ . \tag{2.29}$$

Since the total Hamiltonian $H = H_1 + H_2$ is the sum of independent commuting Hamiltonians operating in their own Hilbert spaces the eigenstates of H are direct products of the eigenstates $|n_1\rangle$ and $|n_2\rangle$, that is

$$\begin{aligned} H|n_1\rangle|n_2\rangle &= \left(H_1|n_1\rangle\right)|n_2\rangle + |n_1\rangle H_2|n_2\rangle \\ &= \left(n_1 + \frac{1}{2}\right)\hbar\omega_1|n_1\rangle|n_2\rangle + \left(n_2 + \frac{1}{2}\right)\hbar\omega_2|n_1\rangle|n_2\rangle \end{aligned} \tag{2.30}$$

i.e., the energy eigenvalues are obtained as a sum of the energy eigenvalues of two harmonic oscillators:

$$E_{n_1,n_2} = \left(n_1 + \frac{1}{2}\right)\hbar\omega_1 + \left(n_2 + \frac{1}{2}\right)\hbar\omega_2\ , \tag{2.31}$$

with frequencies $\omega_1 = \frac{\beta_1\gamma_1}{m^*}$ and $\omega_2 = \frac{\beta_2\gamma_2}{m^*}$.

The energy (2.31) has the following limiting behaviour: at zero magnetic field, the system behaves like a couple of harmonic oscillators in the x and y directions. For a large magnetic field, i.e., when $\omega_c >> \omega_x, \omega_y$, we get $E_{n_x} = \left(n_x + \frac{1}{2}\right)\hbar\omega_c$. The Landau levels are just as in the

case of the isotropic parabolic confinement [1]. When $\omega_x = \omega_y$, i.e., the confinement is isotropic parabolic, $n_x = n + \frac{1}{2}|\ell| - \frac{1}{2}\ell$ and $n_y = n + \frac{1}{2}|\ell| + \frac{1}{2}\ell$, where n and ℓ are the principal and azimuthal quantum numbers respectively. Further, when $\omega_x \approx \omega_y$, the energy levels are very similar to that of the isotropic case except that the $(2n + |\ell| + 1)$ - fold degeneracies at $B = 0$ are lifted [17] as a result of breaking of the circular symmetry. A similar situation also arises when the circular symmetry is broken by the Coulomb coupling between two neighboring dots [18].

Our Hamiltonian thus far describes the spin independent properties of the system but we still have to take care of the spin dependent contributions, namely the Rashba SO coupling and the Zeeman energy, i.e., we need to add to H the operators

$$H_{SO} = \frac{\alpha}{\hbar}\left[\boldsymbol{\sigma} \times \left(\mathbf{p} - \frac{e}{c}\mathbf{A}\right)\right]_z \tag{2.32}$$

and

$$H_z = \frac{1}{2} g \mu_B \mathbf{B} \cdot \boldsymbol{\sigma}, \tag{2.33}$$

where μ_B is the Bohr magneton, and g is the Lande factor. The Zeeman energy represents the coupling of the external magnetic field to the internal magnetic moment of the electron. It splits the Landau levels to spin-up and spin-down sublevels.

2.3 The Fock-Darwin Spectra

In our numerical investigations, we chose the InAs quantum dot with parameters $m^* = 0.042 m_0$, $g = 14$, where m_0 is the free electron mass. The Fock-Darwin states of a single electron in the absence of the SO coupling ($\alpha = 0$) are presented in Fig. 2.1. It shows the magnetic field

dependence of the single-electron energy levels of a quantum dot with $\omega_x = 4$ meV and $\omega_y = 4.1$ meV. For this choice of ω_x and ω_y the deviation from the circular dot is minimal and therefore, as expected, the energy levels are very similar to those of a circular dot [1], except that now the degeneracies are lifted at $B = 0$. As the anisotropy of the QD is increased [Figs. 2.2 – 2.4] along with the shifting of the energy levels to higher energies we also find level splitting at $B = 0$, which are vanishingly small in Fig. 2.1.

Figure 2.1. Fock-Darwin energy levels of an anisotropic quantum dot as a function of the magnetic field B (in Tesla) for $\alpha = 0$ meV nm, $\omega_x = 4$ meV, $\omega_y = 4.1$ meV

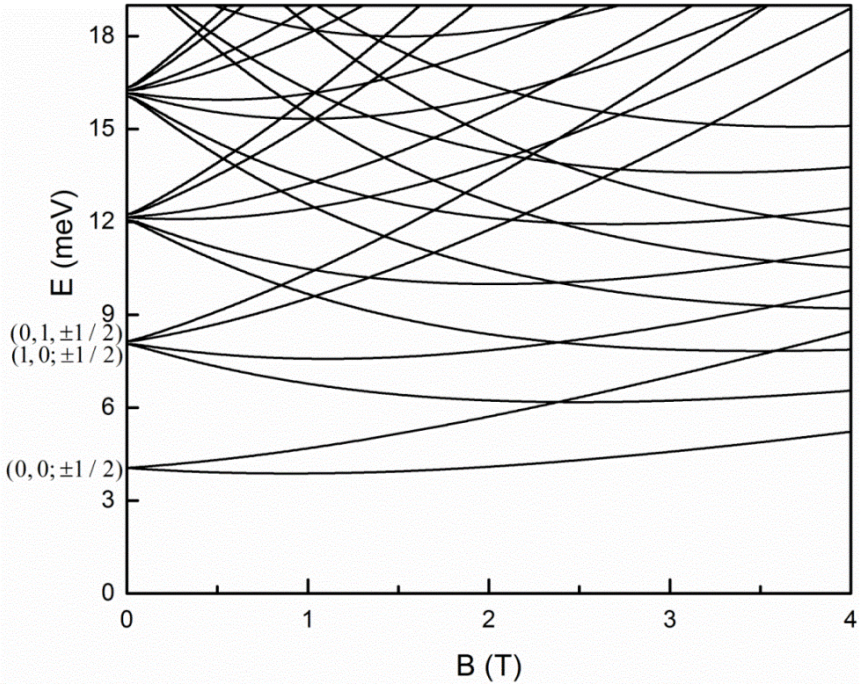

At non-zero magnetic fields the most characteristic feature of the Fock-Darwin levels is their splitting due to the Zeeman coupling into two sublevels corresponding to the spin-up and spin-down states. The separation of these levels increase linearly with the B as $|g\mu_B B|$ (assuming $\mathbf{B} \| \hat{z}$).

Figure 2.2. Fock-Darwin energy levels of an anisotropic quantum dot as a function of the magnetic field B (in Tesla) for $\alpha = 0$ meV nm, $\omega_x = 4$ meV, $\omega_y = 6$ meV.

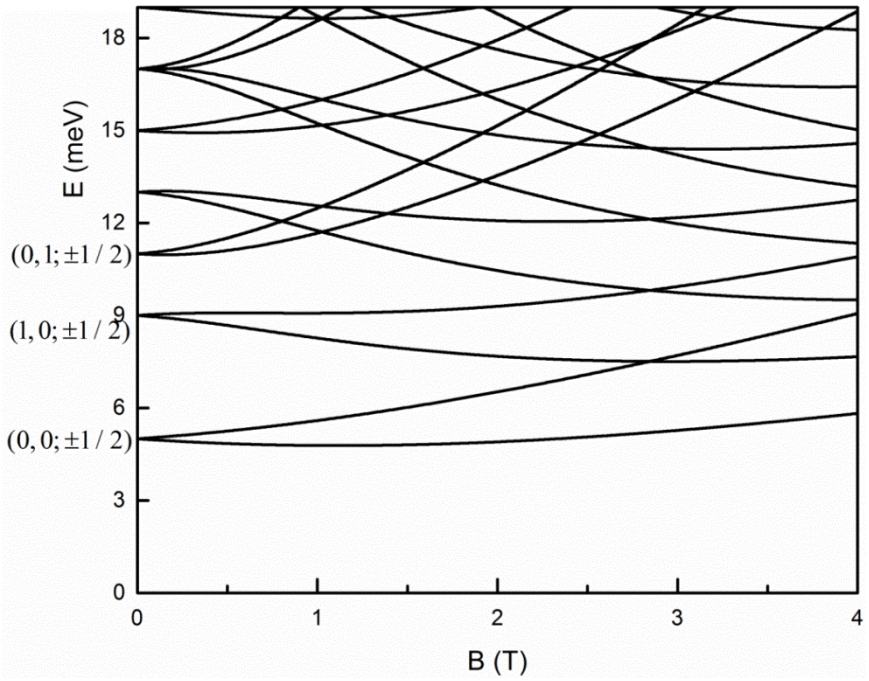

Figure 2.3. Fock-Darwin energy levels of an anisotropic quantum dot as a function of the magnetic field B (in Tesla) for $\alpha = 0$ meV nm, $\omega_x = 4$ meV, $\omega_y = 8$ meV.

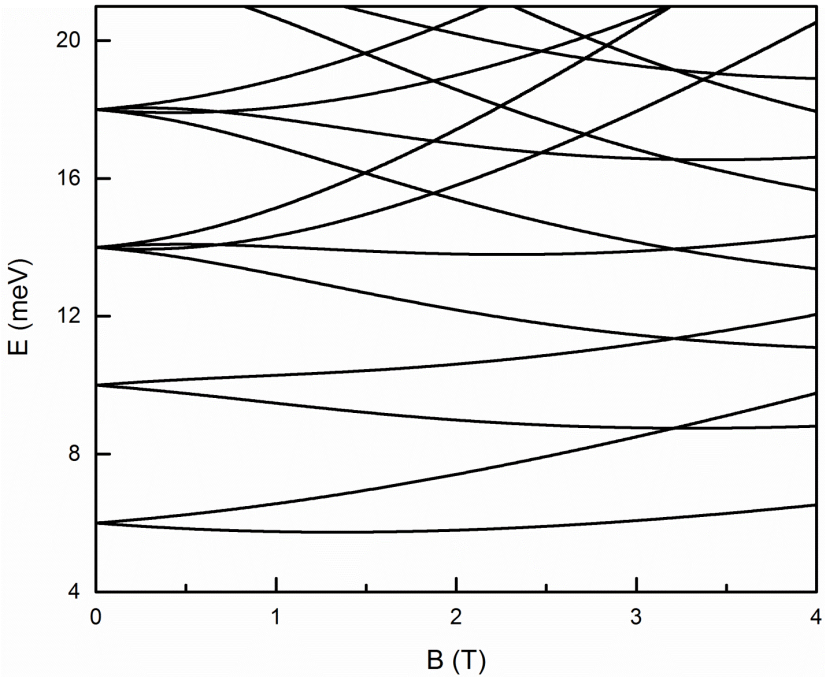

Figure 2.4. Fock-Darwin energy levels of an anisotropic quantum dot as a function of the magnetic field (in Tesla) for $\alpha = 0$ meV nm, $\omega_x = 4$ meV, $\omega_y = 10$ meV.

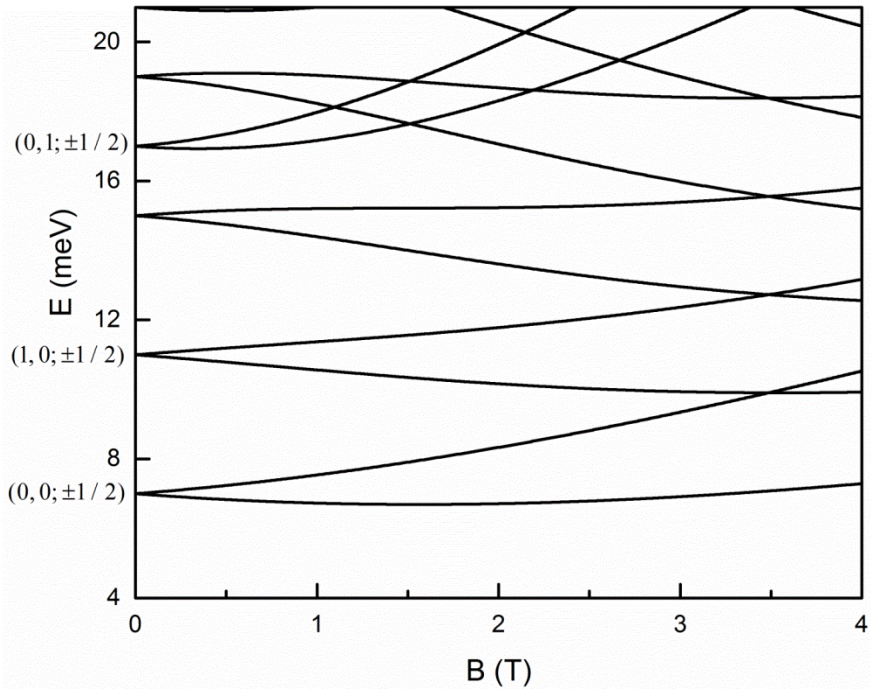

When we are in the limit of a very high magnetic field the spectra go over into that of the Landau levels, as it was in the isotropic case [Fig. 1.1]. The lowest Landau level energy rises with increasing B, but the separation between the energy levels decreases when the magnetic field increases. Therefore, in the limit of $B \to \infty$ the degeneracy in the lowest Landau level becomes very high.

Comparing the energy results in the absence of the SO coupling, it is clearly seen that as ω_y is increased the level crossings are shifted to higher energies. Therefore, we can conclude that the effect of anisotropy itself is to lift the degeneracies of the single-particle spectrum and to shift the level crossings to higher energies.

3 The Rashba Spin-orbit Interaction

The Rashba spin-orbit coupling occurs in quantum structures with asymmetric wells, such as quantum wells formed at the interface between the narrow and wide band-gap semiconductors or in quantum wells with different barrier heights on the two sides. A gradient in the potential energy profile is thereby created with an electric field that can be tuned by an applied gate voltage. An electron moving in the well sees this field as an effective magnetic field in the plane of the electron gas and perpendicular to the electric field. This effective magnetic field creates the spin-orbit coupling, and lifts the spin degeneracy. The energy dispersion relation for the Rashba Hamiltonian (2.32) for a two-dimensional electron gas is

$$E_{\mathbf{k}} = \frac{\hbar^2 k^2}{2m^*} \pm \alpha k \,, \tag{3.1}$$

where the first term is the kinetic energy of the electron. The SO coupling parameter α depends on the details of the quantum well, but can be controlled by an externally applied gate voltage. The Rashba spin splitting $\Delta = 2\alpha k$, occurs even in the absence of an external magnetic field. A schematic plot of the dispersion relation is presented in Fig. 3.1 (in one dimension) which consists of two parabolas that are shifted horizontally with respect to each other. Electrons with opposite spins travel with different Fermi velocities and therefore have two different wave vectors. This results in a beating pattern in the Shubnikov-de-Haas oscillations which is experimentally measured to determine α [19, 20]. The opposite spin energies are shifted along $\mathbf{k}$, unlike in the case of Zeeman interaction (2.33) where the splitting is vertical (along the energy axis).

Figure 3.1. Energy dispersion curves for the Rashba SO coupling Hamiltonian in one dimension.

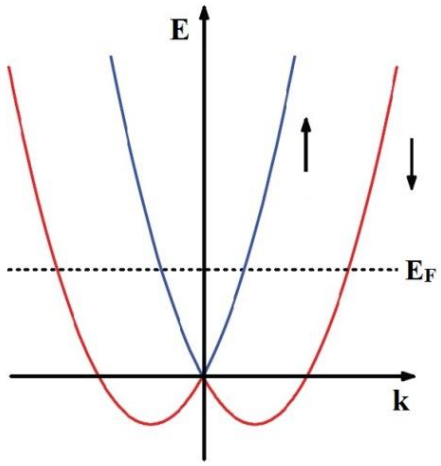

In general, the spin-orbit interaction (SOI) couples the spin degree of freedom with the orbital motion of an electron. The latter is strongly dependent on the choice of the confinement potential. Hence it is important to investigate how the interplay between the SOI and the confinement potential modifies the quantum states of electrons in nanostructures. The SOI in semiconductor nanostructures originates from breaking of the inversion symmetry and in materials where the structural inversion symmetry breaking is dominant, e.g., in InAs, the SOI is largely described by the Rashba Hamiltonian described below.

Of late, the spin-orbit coupling in semiconductor nanostructures [21] is receiving increasing attention, largely due to the prospect of possible realization of coherent spin manipulation in spintronic devices [15], where the SOI is destined to play a crucial role [5,15]. As the SOI couples the orbital motion of the charge carriers with their spin state, an all-electrical control of the spin states in nanoscale semiconductor devices could thus be a reality. In this context, the Rashba SOI [6] has received particular attention because in a two-dimensional electron gas the strength of the Rashba SOI can be tuned by the application of an electric field [22, 23]. While the earlier studies of Rashba spin-orbit coupling were primarily in a two-dimensional electron gas

[5], we have concentrated on the role of SOI in a single InAs quantum dot. Chakraborty and Pietiläinen [10] have reported extensive theoretical studies about the influence of the Rashba SOI on the energy spectrum for circularly symmetric parabolic confinement. There the SO coupling was found to manifest itself mainly in multiple level crossings and level repulsions. Those were attributed to the interplay between the Zeeman and the SO interactions present in the system Hamiltonian. However, those effects, in particular the level repulsions, were weak and as a result it would require extraordinary efforts to detect the strength of the SO coupling [11] in circularly symmetric, isotropic quantum dots. Introducing anisotropy in a QD [14], we have shown that a major enhancement of the Rashba SO coupling effects can be generated in the system. This can be observed directly in the Fock-Darwin states of a QD, and therefore should be experimentally observable [1,2]. We find that the Rashba SO coupling effects are manifestly strong in an elliptical QD [14], which should provide a direct route to determine and control the SO coupling strength. The anisotropy of a quantum dot can in turn be tuned by an in-plane magnetic field, as has been proposed in Ref. [24].

3.1 The Rashba Hamiltonian

The Hamiltonian describing the spin-orbit interaction in our system is [10]

$$H_{SO} = \frac{\alpha}{\hbar}\left[\boldsymbol{\sigma} \times \left(\mathbf{p} - \frac{e}{c}\mathbf{A}\right)\right]_z = \frac{\alpha}{\hbar}\left[\sigma_x\left(p_y - \frac{e}{c}A_y\right) - \sigma_y\left(p_x - \frac{e}{c}A_x\right)\right]. \tag{3.2}$$

To handle the SO coupling we need to incorporate also the spin degree of freedom into the states, discussed in Sect. 2. We do this by attaching a third quantum number, related to the orientation of electron spin, to the basic oscillator states such that

$$\left|n_1, n_2; s_z\right\rangle = \left|n_1, n_2\right\rangle\left|s_z\right\rangle, \tag{3.3}$$

where the quantum number s_z takes the values ± 1, and the state $|s_z\rangle$ stands for the spinors

$$\begin{aligned} |+1\rangle &= |\uparrow\rangle = \begin{pmatrix} 1 \\ 0 \end{pmatrix} \\ |-1\rangle &= |\downarrow\rangle = \begin{pmatrix} 0 \\ 1 \end{pmatrix} \end{aligned} \tag{3.4}$$

Recalling that for the vector potential we chose the symmetric gauge $\mathbf{A} = \frac{1}{2} B(-y, x, 0)$, for the SO operator we find that

$$\begin{aligned} \frac{\hbar}{\alpha} H_{SO} &= \sigma_x \left(p_y - \frac{eB}{2c} x \right) - \sigma_y \left(p_x + \frac{eB}{2c} y \right) \\ &= \sigma_x \left(\sin\chi\, \chi_1 - \cos\chi\, \omega_0 \right) q_1 \\ &- \sigma_y \left(\sin\chi\, \chi_1 + \cos\chi\, \omega_0 \right) q_2 \\ &- \sigma_y \left(\cos\chi - \sin\chi\, \omega_0\, \chi_2 \right) p_1 \\ &+ \sigma_x \left(\cos\chi + \sin\chi\, \omega_0\, \chi_2 \right) p_2, \end{aligned} \tag{3.5}$$

where $\omega_0 = eB/2c$. The operator H_{SO} is Hermitian as can be proved by calculating the matrix elements of the SO operator [Appendix B.2]. The effect of the SO coupling is handled by resorting to the standard ladder operator formalism of the harmonic oscillators and by diagonalizing H_{SO} in the complete basis formed by the vectors $|n_1, n_2; s_z\rangle$.

3.2 Computational Scheme

Since H_{SO} is a Hermitian operator, its matrix representation $\langle n_1', n_2'; s_z' | H_{SO} | n_1, n_2; s_z \rangle$ is also Hermitian. The size of the basis, and hence the dimension of the Hamiltonian matrix has to be large enough to ensure the convergence of the state vectors we are interested in. As we present only a few low-lying energy levels in the results below, the dimensions of the Hermitian matrix

is at most a few hundred. This makes the full diagonalization a relatively fast job. With the material parameters and the confinement potential strength as input, we take the following steps in obtaining the numerical results presented in this thesis.

For each value of the magnetic field B,

i. The basis consisting of the states $|\lambda\rangle = |n_1, n_2; s_z\rangle$ is constructed in energetically ascending order. The quantum numbers n_i refer to the two one-dimensional oscillators with the canonical coordinates q_i and p_i, and s_z to the direction of the electron spin. The size of the basis is determined such that the desired accuracy in later stapes is achieved.

ii. The Hermitian matrix with the elements $\langle \lambda' | H_{SO} | \lambda \rangle$ is constructed and diagonalized. This results in the energy spectrum and the eigenvectors which describe the SO coupled one-electron states $|n\rangle$. Since the dimension of this matrix is at most of the order of hundreds, a full diagonalization using a standard algorithm is perfectly feasible.

iii. The quantities $\langle 0|x|n\rangle$ needed for the absorption cross section [Sect. 4.1] of the transition from the ground state $|0\rangle$ to the excited states $|n\rangle$ are obtained as

$$\langle 0|x|n\rangle = \sum_{\lambda'\lambda} \left(C^0_{\lambda'}\right)^* C^n_\lambda \langle \lambda'|x|\lambda\rangle$$

where C^i_λ are the components of the eigenvector representing a SO coupled eigenstate $|i\rangle$ obtained in step ii. Similar procedure is applied to the dipole term $\langle 0|y|n\rangle$.

3.3 The Fock-Darwin Spectra with the Spin-orbit Interaction

Let us now take a look at the energy spectra of an anisotropic QD in the presence of the spin-orbit coupling to find out how they differ from those without the SOI. In Figs. 3.2 – 3.5 we presented the Fock-Darwin states with the SOI included (α = 20 meV nm) for ω_x = 4 meV and ω_y = 4.1, 6, 8, 10 meV, respectively. These results demonstrate that many excited states retain their degeneracy no matter how strong the SOI is or how eccentric the dot is. At the same time, many other degeneracies are removed by squeezing or stretching the dot. At non-zero magnetic fields some of the crossings of the energy spectra are turned to anticrossings by the Rashba term in the Hamiltonian. For example, the second and third excited states are mainly composed of the states $|0,0;1/2\rangle$ and $|1,0;-1/2\rangle$ (marked as ● and ⊗ in Fig. 3.2, respectively), which are mixed by the H_{SO} around B = 3 Tesla, causing a level repulsion.

Figure 3.2 Magnetic field (in Tesla) dependence of the low-lying Fock-Darwin energy levels of an elliptical dot with the Rashba SOI for α = 20 meV nm, ω_x = 4 meV, ω_y = 4.1 meV

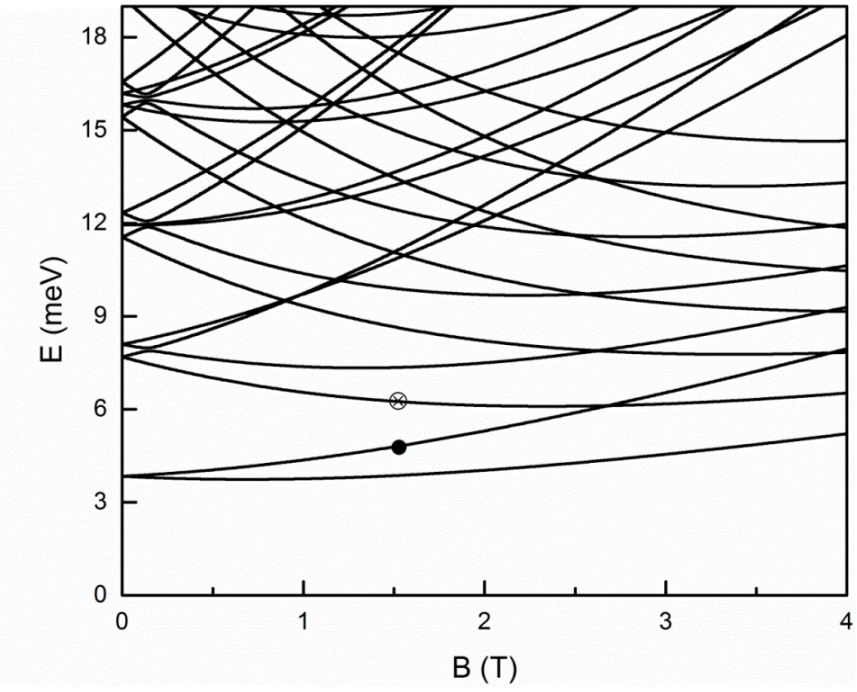

Figure 3.3 Magnetic field (in Tesla) dependence of the low-lying Fock-Darwin energy levels of an elliptical dot with Rashba SOI for $\alpha = 20$ meV nm, $\omega_x = 4$ meV, $\omega_y = 6$ meV

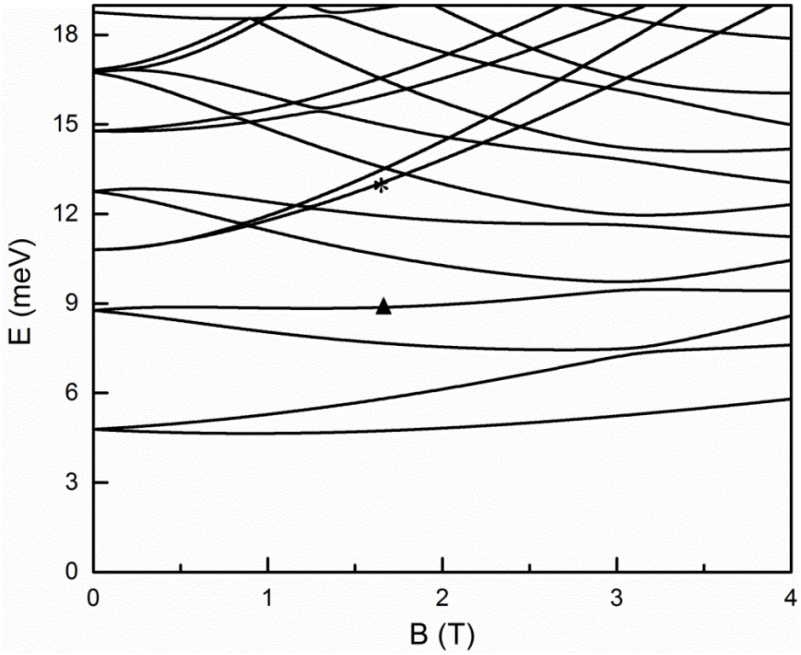

Figure 3.4 Magnetic field (in Tesla) dependence of the low-lying Fock-Darwin energy levels of an elliptical dot with Rashba SOI for $\alpha = 20$ meV nm, $\omega_x = 4$ meV, $\omega_y = 8$ meV

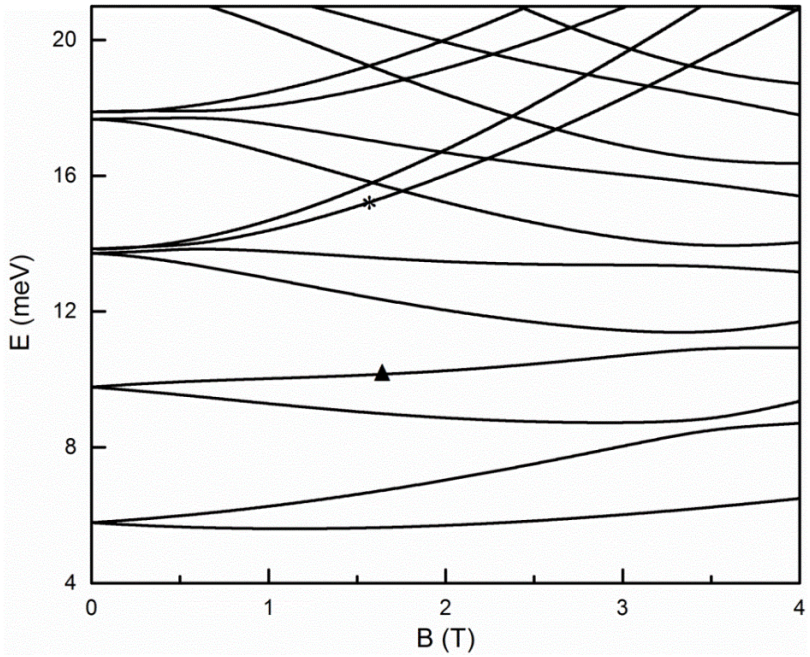

Figure 3.5 Magnetic field (in Tesla) dependence of the low-lying Fock-Darwin energy levels of an elliptical dot with Rashba SOI for $\alpha = 20$ meV nm, $\omega_x = 4$ meV, $\omega_y = 10$ meV

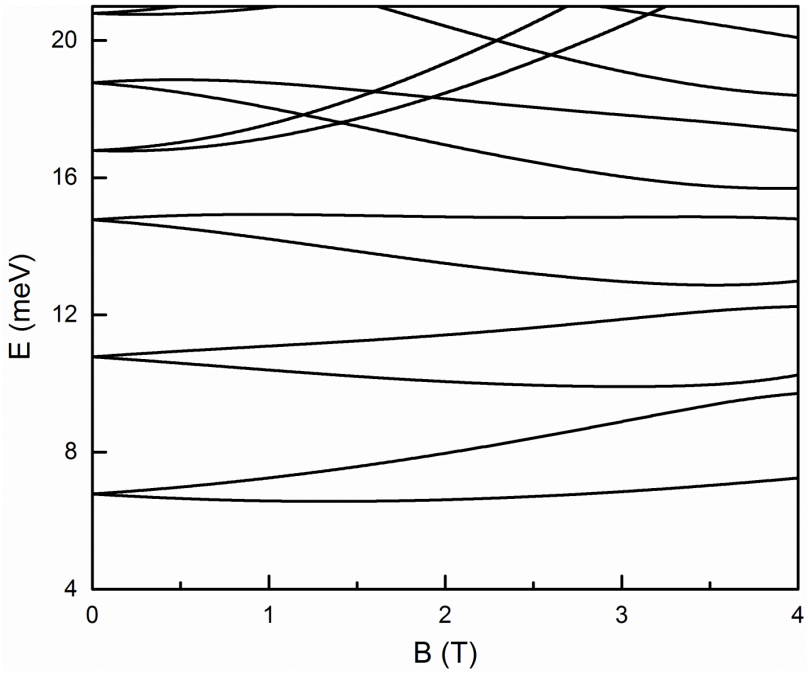

When compared to the Fock-Darwin spectra of anisotropic quantum dots without the SO coupling (shown in Figs. 2.1 – 2.4), the most outstanding features in the energy spectra of the elliptical QDs with the spin-orbit coupling are the rearrangement of some of the levels at the small field and level repulsions at higher magnetic fields.

Squeezing of the dot also enhances the SO coupling. The level repulsion gap due to the Rashba SOI is presented in Fig. 3.6 as a function of ω_y, while ω_x is kept fixed at 4 meV. Only the lowest two level repulsion gaps, around the magnetic field of B = 3-4 Tesla, are shown. It is clearly seen, in both cases, that there is a rapid increase of the gap as a function of the eccentricity. Such a prominent effect of Rashba has not been found before.

Figure 3.6 The Rashba gap for the lowest level repulsion (1st gap) and for the next higher energy (2nd gap) versus the anisotropy of the dot

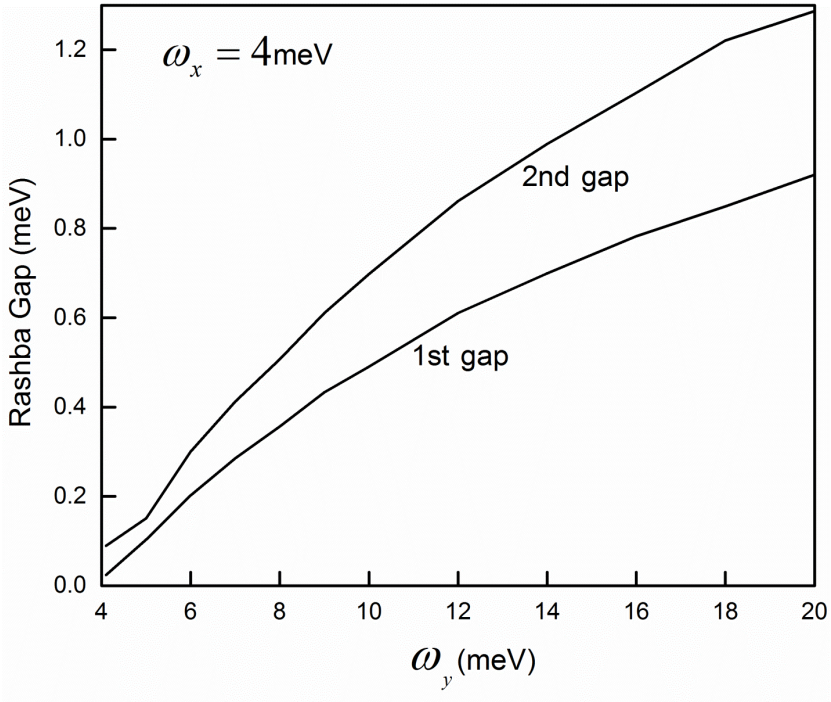

In fact, the four lowest gaps shown in Figs. 3.2 - 3.5 at around 3 – 4 Tesla are between the states with major components $|n, 0; 1/2\rangle$ and $|n+1, 0; -1/2\rangle$, that is, between the states related to the oscillations (approximately) parallel to the x axis. When the dot is squeezed in the y direction we would expect these states to experience only the trivial zero-point-energy shift of the magnitude $\frac{1}{2}\hbar\Delta\omega_y$. In particular, we would expect the Rashba gap to approximately retain its width. There are, however, two indirect mechanisms that are influencing the size of the gap. The first one can be understood using the simple perturbation-theoretical arguments: the squeezing moves the states $|n+1, 1; 1/2\rangle$ to such high energies that their tendency to repel the states $|n+1, 0; -1/2\rangle$ downward and to close the gap is diminished. The second mechanism is attributed to the imposed magnetic field which rotates the oscillators in the phase space by

mixing the high-momentum y direction oscillation with the x direction motion. Since the SO interaction is proportional to the momentum, this mixing will increase the Rashba effect.

4 Dipole - allowed Transitions

Far-infrared (FIR) magneto-optical absorption spectroscopy has been a very useful experimental technique where one studies the electron excitations to higher energy states. In the case of circular QDs the absorption spectrum was found to be deceptively simple [1, 2, 25]. At $B = 0$, there is only one resonance which splits into two modes as the magnetic field is increased. Interestingly, the spectrum is independent of the number of electrons. This interesting but puzzling observation was explained [1] by noticing that for the parabolic confinement potential the dipole transitions correspond to the centre of mass motion, while the relative motion that describes the collective excitations of electrons in the QD remains unchanged. This situation can however be altered by introducing a non-parabolic confinement [26], or for anisotropic QDs. Spin-orbit interaction can also influence the FIR spectrum of the QDs [10].

4.1 The Absorption Cross Section

The effects of anisotropy and spin-orbit interaction on the energy spectra presented above are also reflected in the optical absorption spectra. Let us now turn our attention to the absorption spectra for transitions from the ground state to the excited states. For that purpose we subject the dot to the radiation field

$$\mathbf{A}_R = A_0 \hat{\boldsymbol{\varepsilon}} \left(\exp(i(\omega / \mathrm{c}) \hat{\mathbf{n}} \cdot \mathbf{r} - i\omega t) + \exp(-i(\omega / \mathrm{c}) \hat{\mathbf{n}} \cdot \mathbf{r} + i\omega t) \right), \tag{4.1}$$

where $\hat{\boldsymbol{\varepsilon}}$, ω and $\hat{\mathbf{n}}$ are the polarization, frequency and direction of propagation of the incident light, respectively. We let the radiation enter the dot along the direction perpendicular to the

motion of the electron, that is, parallel to the z axis. Due to the transversality condition $(\nabla \cdot \mathbf{A}_R = 0)$ the polarization vector will then lie in the xy plane. We now assume that the intensity of the field is so weak that only the terms linear in A_R have to be taken into account. Then the effect of the radiative magnetic field on the spin can be neglected as well. So we can replace in the Hamiltonian H the vector potential A with the field $A' = A + A_R$. Discarding terms higher than linear order in A_R, we get the total Hamiltonian $H' = H + H_R$, with the radiative part

$$H_R = -\frac{e}{m^* c}\mathbf{A}_R \cdot \left(\mathbf{p} - \frac{e}{c}\mathbf{A}\right) - \frac{\alpha e}{\hbar c}\left[\boldsymbol{\sigma} \times \mathbf{A}_R\right]_z . \tag{4.2}$$

Dipole approximation: We assume that the amplitude of radiation can be taken as constant within the dot, so that the field is written as $\mathbf{A}_R \approx A_0 \hat{\boldsymbol{\varepsilon}}\left(\exp(-\mathrm{i}\omega \mathrm{t}) + \exp(\mathrm{i}\omega \mathrm{t})\right)$. Since the transition energies expressed in terms of radiation frequencies are of the order of terahertz, the corresponding wavelengths are much larger than the typical size of a dot, thus justifying our approximation. As a result, H_R can be written as

$$H_R = -\left[\frac{eA_0}{m^* c}\hat{\boldsymbol{\varepsilon}} \cdot \left(\mathbf{p} - \frac{e}{c}\mathbf{A}\right) + \frac{\alpha e A_0}{\hbar c}\left[\boldsymbol{\sigma} \times \hat{\boldsymbol{\varepsilon}}\right]_z\right]\left(\exp(-\mathrm{i}\omega \mathrm{t}) + \exp(\mathrm{i}\omega \mathrm{t})\right). \tag{4.3}$$

When $\alpha = 0$ the first term generates the center of mass density excitation, consequently (in dipole approximation) only transitions between these modes are possible. When α is different from zero, the second term $(\sigma_x \varepsilon_y - \sigma_y \varepsilon_x)$ in H_R can create spin-density oscillations.

The Fermi golden rule now leads to the dipole approximation form

$$\sigma_{abs}(\omega) = 4\pi^2 \alpha_F \, \omega_{ni} \left|\langle n | \hat{\boldsymbol{\varepsilon}} \cdot \mathbf{r} | i \rangle\right|^2 \delta(\omega_{ni} - \omega) \tag{4.4}$$

of the absorption cross section for transitions from the initial state $|i\rangle$ to the final state $|n\rangle$. Here $\alpha_F = \frac{e^2}{\hbar c} = \frac{1}{137}$ is the fine structure constant and ω_{ni} is the frequency corresponding to the transition energy $\hbar\omega$. Since we look at the radiation entering the dot along the z direction, the polarization vector $\hat{\boldsymbol{\varepsilon}}$ lies in the xy plane, i.e., we can write

$$\hat{\boldsymbol{\varepsilon}} = \cos\gamma\,\mathbf{i} + \sin\gamma\,\mathbf{j}. \tag{4.5}$$

The absorption cross section is then written

$$\sigma_{abs}(\omega) = 4\pi^2\alpha_F\,\omega_{ni}\left|\cos\gamma\langle n|x|i\rangle + \sin\gamma\langle n|y|i\rangle\right|^2\delta(\omega_{ni}-\omega) \tag{4.6}$$

where γ is the polarization angle with respect to the original unrotated x axis.

We should point out here that the absorption cross section formula (4.6) remains valid in the SO coupled systems as well. This can be easily verified by evaluating its commutator with the Hamiltonian H

$$\begin{aligned}\left[x,H\right] &= i\frac{\hbar}{m^*}\left(\mathbf{p}-\frac{e}{c}\mathbf{A}\right)_x - i\alpha\sigma_y \\ \left[y,H\right] &= i\frac{\hbar}{m^*}\left(\mathbf{p}-\frac{e}{c}\mathbf{A}\right)_y - i\alpha\sigma_x.\end{aligned} \tag{4.7}$$

For the expression (4.4) the commutation relation is

$$\left[\hat{\boldsymbol{\varepsilon}}\cdot\mathbf{r},H\right] = -i\hbar H_R\frac{c}{eA_0}\left(\exp(-\mathrm{i}\,\omega\,\mathrm{t}) + \exp(\mathrm{i}\,\omega\,\mathrm{t})\right)^{-1}. \tag{4.8}$$

This implies that finding the matrix elements of H_R is equivalent to finding just the matrix elements of $\langle n|\hat{\boldsymbol{\varepsilon}}\cdot\mathbf{r}|i\rangle$

$$\langle n|H_R|i\rangle \simeq \langle n|[\hat{\boldsymbol{\varepsilon}}\cdot\mathbf{r},H]|i\rangle = \langle n|\hat{\boldsymbol{\varepsilon}}\cdot\mathbf{r}|i\rangle\left(\hbar\omega_n - \hbar\omega_i\right) = \hbar\omega_{ni}\langle n|\hat{\boldsymbol{\varepsilon}}\cdot\mathbf{r}|i\rangle \tag{4.9}$$

where we have used the fact that $|i\rangle$ and $|n\rangle$ are the eigenstates of H with eigenvalues $E_i = \hbar\omega_i$

and $E_n = \hbar\omega_n$, and that due to the energy conservation we have $\omega_{ni} = \omega_n - \omega_i$. Consequently for the absorption cross section we have the expression given by (4.4).

4.2 The Dipole Transition Matrix Elements

To evaluate the cross sections we need the matrix elements of the original coordinates

$$\begin{aligned} x &= q_1 \cos\chi - \chi_2\ p_2 \sin\chi \\ y &= q_2 \cos\chi - \chi_2 p_1 \sin\chi. \end{aligned} \tag{4.10}$$

For that purpose we need to know the matrix elements of q_i and p_i. The task becomes much easier when we express the position and momentum operators in terms of the ladder operators:

$$\begin{aligned} q_i &= \sqrt{\frac{\hbar}{2m_i\omega_i}}\left(\mathrm{a}_i + \mathrm{a}_i^\dagger\right) = \sqrt{\frac{\hbar}{2}}\,\frac{1}{\kappa_i}\left(\mathrm{a}_i + \mathrm{a}_i^\dagger\right) \\ p_i &= i\sqrt{\frac{\hbar m_i\omega_i}{2}}\left(\mathrm{a}_i^\dagger - \mathrm{a}_i\right) = i\sqrt{\frac{\hbar}{2}}\,\kappa_i\left(\mathrm{a}_i^\dagger - \mathrm{a}_i\right) \end{aligned} \tag{4.11}$$

where $\kappa_i^2 = m_i\omega_i = \frac{\gamma_i}{\beta_i}$.

The matrix elements of the ladder operators for the eigenstates of the Hamiltonian are calculated as

$$\begin{aligned} \left\langle n_1', n_2' \,|\, a_1 \,|\, n_1, n_2 \right\rangle &= \left\langle n_1' \,|\, a_1 \,|\, n_1 \right\rangle \left\langle n_2' \,|\, n_2 \right\rangle = \sqrt{n_1}\,\delta_{n_1', n_1 - 1}\delta_{n_2', n_2} \\ \left\langle n_1', n_2' \,|\, a_1^\dagger \,|\, n_1, n_2 \right\rangle &= \left\langle n_1' \,|\, a_1^\dagger \,|\, n_1 \right\rangle \left\langle n_2' \,|\, n_2 \right\rangle = \sqrt{n_1 + 1}\,\delta_{n_1', n_1 + 1}\delta_{n_2', n_2} \\ \left\langle n_1', n_2' \,|\, a_2 \,|\, n_1, n_2 \right\rangle &= \sqrt{n_2}\,\delta_{n_1', n_1}\delta_{n_2', n_2 - 1} \\ \left\langle n_1', n_2' \,|\, a_2^\dagger \,|\, n_1, n_2 \right\rangle &= \sqrt{n_2 + 1}\,\delta_{n_1', n_1}\delta_{n_2', n_2 + 1}. \end{aligned} \tag{4.12}$$

These relations make it easy to determine the matrix elements of q_i and p_i [Appendix B.1], and then the matrix elements of the conventional position and momentum operators x, y and $p_{x,y}$ (details can be found in Appendix B.3).

4.3 The Selection Rules

The dipole-allowed optical transitions are always between the same spin states and the principal quantum number n_1 or n_2 changed by unity. This can be seen by calculating the dipole transition matrix elements [1] [Appendix B.3]. When the polarization is along the x or y axis, we have $\Delta n_1 = 0,\ \Delta n_2 = \pm 1$ or $\Delta n_1 = \pm 1,\ \Delta n_2 = 0$. This means that there are just two transition modes as in the case of isotropic parabolic confinement [1]. In the presence of the SO coupling, neither the dipole operator nor the selection rules change, but the SOI mixes the states which differ in spin orientation, and differ by 1 either in the quantum number n_1 or n_2, but not in both. For rotationally symmetric confinements, these selection rules apply to the conservation of the total angular momentum J in the planar motion of the electron. Therefore, in the presence of the SO coupling, transitions from other states that are not allowed when $\alpha = 0$, should now become observable.

4.4 The Absorption Spectra

We now show that the absorption cross sections for the dipole allowed transitions [14] from the ground states corresponding to the energy spectra above in Sect. 2 and Sect. 3. To evaluate the cross sections we use Eq. (4.4). Computation of the matrix element of this polarization operator between the ground state and the excited states of the Hamiltonian yields transition amplitudes

for the absorption. The absorption depends on the polarization since in elliptical dots the oscillation strengths

$$f_{ni} = \frac{2m^{*}\omega_{ni}}{\hbar}\left|\langle n|\hat{\boldsymbol{\varepsilon}}\cdot\mathbf{r}|i\rangle\right|^{2} \tag{4.13}$$

probe the occupations of the quantum states related to the oscillations in the direction of the polarization $\hat{\boldsymbol{\varepsilon}}$. In a circular dot all oscillation directions are equally probable at all energies, implying that the oscillator strengths are independent of the polarization and depend only on the transition energy via the ω_{ni}, and the final-state quantum numbers $n_{1,2}$ [see Fig. 4.1]. The absorption spectra is almost the same for an almost circularly symmetric quantum dot, i.e., when we have a small anisotropy in the dot [Fig 4.2]. However, by increasing the anisotropy of the dot we found new features in the transition spectrum [14]. When the dot is squeezed in the y direction, the oscillator states related to the y axis motion are pushed up in energy. The polarization being along the x axis, most of the oscillator strength comes from transitions to the allowed states with the lowest energies. Similarly, when the incident radiation is polarized along the y axis most of the contribution is due to the transitions to the oscillator states pushed up in energy. Furthermore, the phase-space rotation formula [Eq. (2.12)] show that the external magnetic field tends to rotate the directions of the oscillator motion, causing a shift of the oscillator strength from one allowed transition to another. This is precisely what is seen in Figs. 4.3 (a) and 4.3 (b).

Figure 4.1. Absorption spectra for circularly symmetric quantum dot versus the magnetic field B (in Tesla): $\alpha = 0$ meV nm, $\omega_x = \omega_y = 4$ meV. The size of the filled dot is proportional to the calculated intensity.

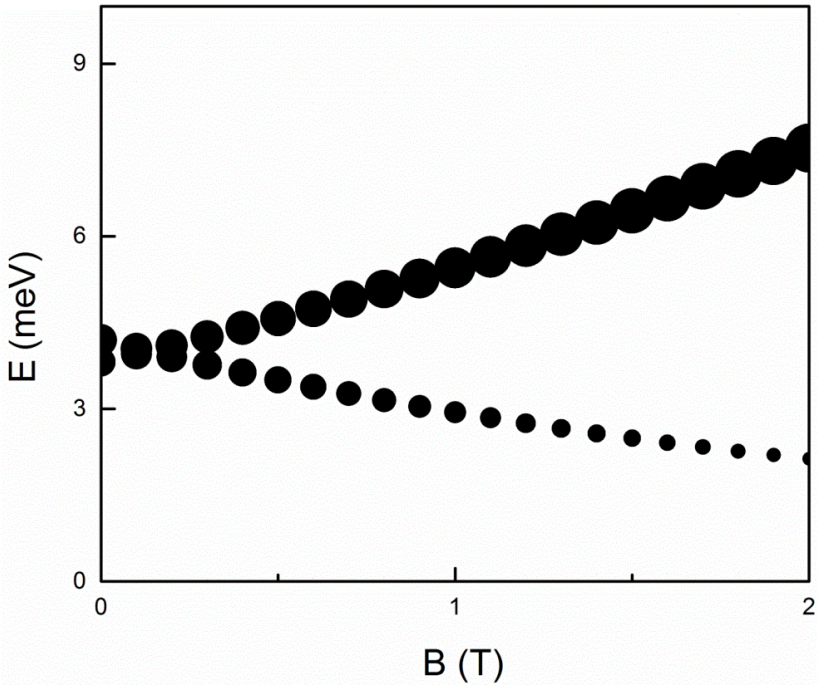

Figure 4.2. Absorption spectra for an almost circular dot versus the magnetic field B (in Tesla): $\alpha = 0$ meV nm, $\omega_x = 4$ meV, $\omega_y = 4.1$ meV. The size of the filled dot is proportional to the calculated intensity.

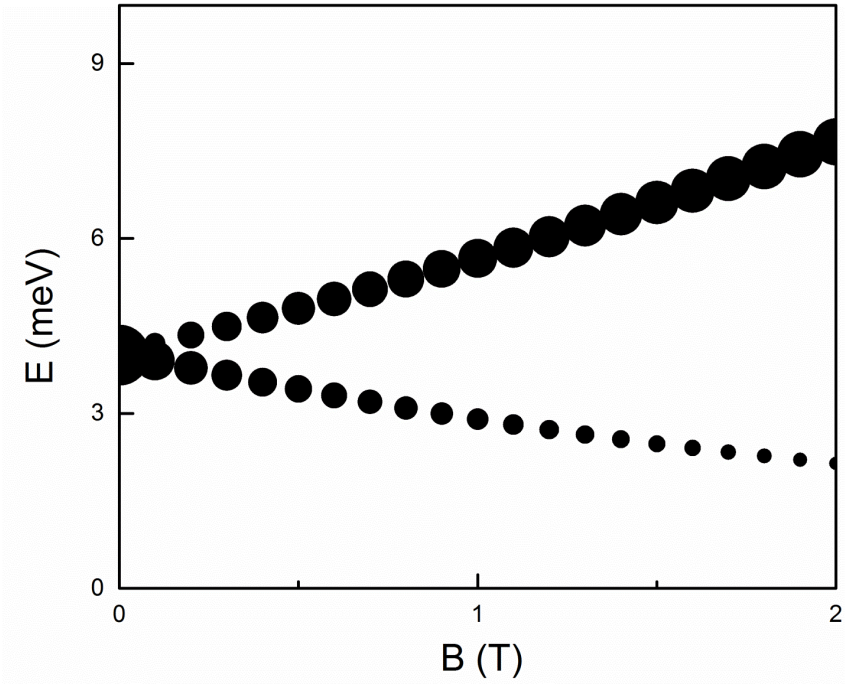

In Fig. 4.3 (a) the polarization of the incident radiation is along the x axis and we notice that most transitions are from the states with lower energies, whereas in Fig. 4.3 (b) the incident radiation is polarized along the y axis and because the y-polarization probes for oscillations along the y direction the related transitions go mostly to the upper mode. The resulting transitions are therefore super-intense, unlike in isotropic QDs. The areas of the filled circles are proportional to the calculated absorption cross section (4.2).

The dipole selection rules for the oscillator states are also largely followed in Fig. 4.3. These rules – the spin state is preserved and either n_1 or n_2 is changed by unity – fully determine the two allowed transitions $|0,0;-1/2\rangle \to |1,0;-1/2\rangle$ and $|0,\,0;\,-1/2\rangle \to |0,\,1;\,-1/2\rangle$ in Fig 2.1. Even in the presence of the spin-orbit interaction the two allowed final oscillator states provide the major contributions to the corresponding SOI included states. Hence, we still see two dominant absorption lines. However, now many other transitions are also allowed [Fig. 4.4].

Figure 4.3 Optical absorption (dipole-allowed) spectra of elliptical QD versus the magnetic field B (in Tesla) for x and y polarizations: $\alpha = 0$ meV nm, $\omega_x = 4$ meV, $\omega_y = 6$ meV. The size of the filled dot is proportional to the calculated intensity

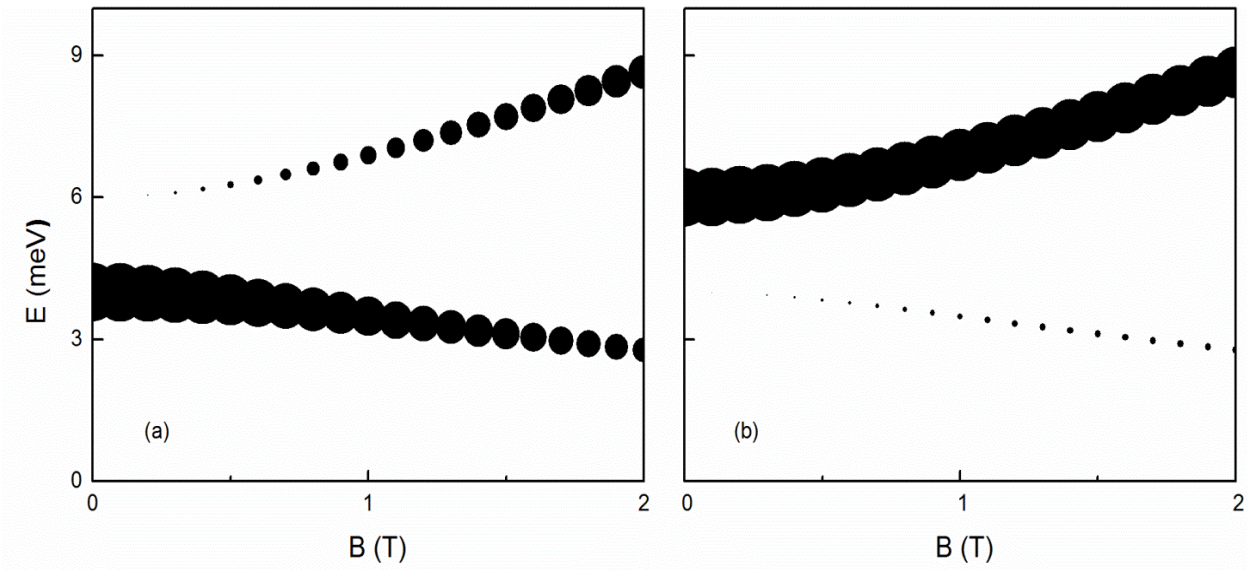

The lowest absorption line corresponding to the transition between the Zeeman-split states with the main components $|0, 0; -1/2\rangle$ and $|0, 0; 1/2\rangle$ provides a typical example. The transition involves a spin flip and is therefore strongly forbidden without the spin-orbit interaction. As the SOI mixes the state $|1, 0; 1/2\rangle$ [marked as ▲ in Fig. 3.3] with the former and $|0, 1; -1/2\rangle$ [marked as ∗ in Fig. 3.3] with the latter, the transition is allowed. The appearance of other new lines can be explained by analogous arguments. For larger Rashba coupling we also see additional features involving discontinuities and anticrossings in Fig. 4.5, which are the consequences of the anticrossings present in the energy spectra.

Figure 4.4. Optical absorption (dipole-allowed) spectra of elliptical QD versus the magnetic field B (in Tesla) in the presence of the SO coupling, for x and y polarizations: $\alpha = 20$ meV nm, $\omega_x = 4$ meV, $\omega_y = 8$ meV. The size of the dot is proportional to the calculated intensity

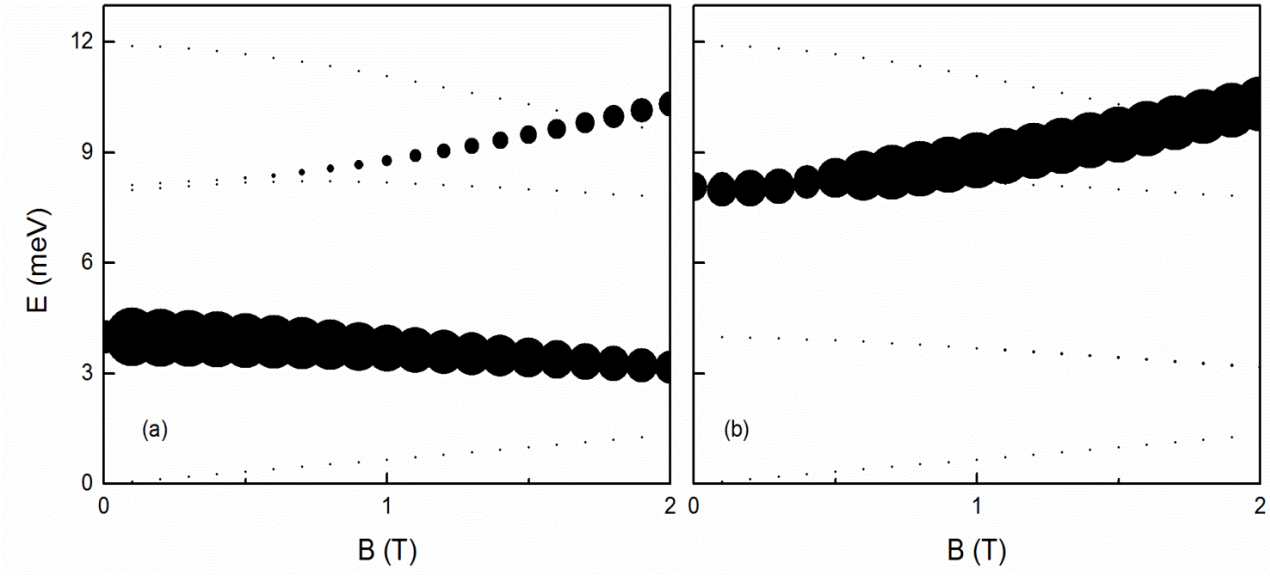

Figure 4.5. Optical absorption (dipole-allowed) spectra of the elliptical QD versus the magnetic field B (in Tesla) in the presence of the SO coupling, for x and y polarizations: $\alpha = 40$ meV nm, $\omega_x = 4$ meV, $\omega_y = 6$ meV. The size of the filled dot is proportional to the calculated intensity

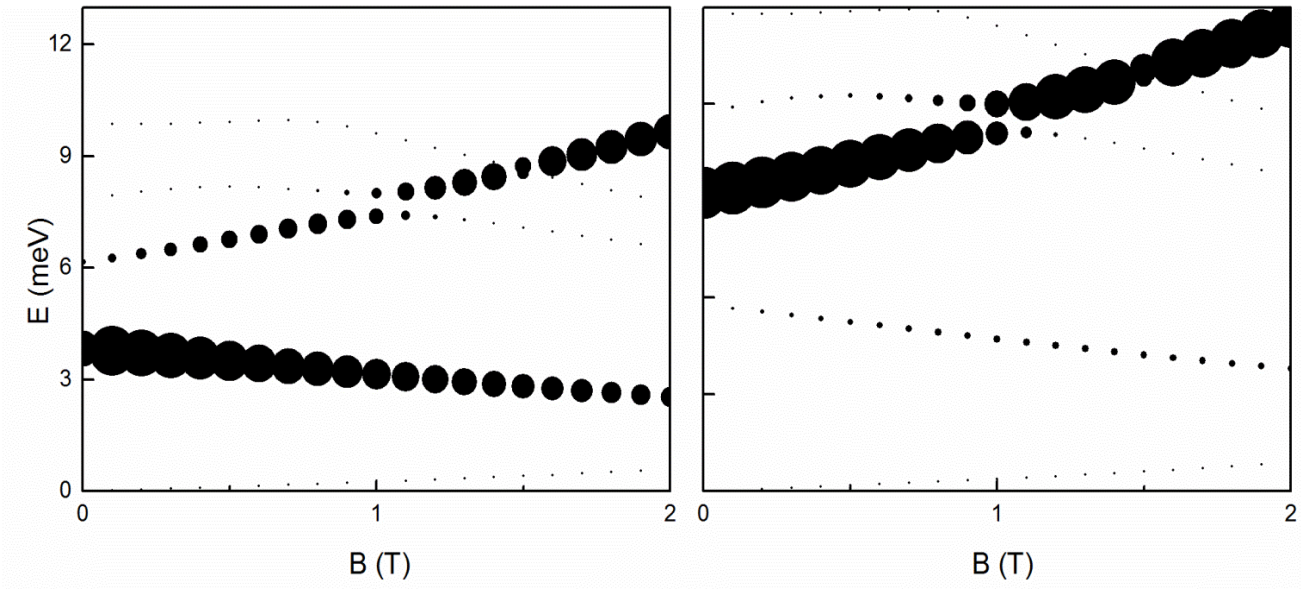

The oscillator strengths satisfy the Thomas-Reiche-Kuhn sum rule [27]: $\sum_n f_{ni} = 1$. In terms of the cross section this translates to the condition

$$\int_{-\infty}^{\infty} \sigma_{abs}(\omega)\,\mathrm{d}\omega = \frac{2\pi^2\hbar\alpha_F}{m^*}. \tag{4.14}$$

The absorptions in Figs. 4.3 - 4.5 practically saturate the sum rule[1], the saturation being, of course complete in the absence of the SOI in Figs. 4.2 and 4.3. The largest fraction of the cross section either falling outside of the displayed energy scale or having too low intensity to be discernible in our pictures is found at the strongest Rashba coupling in Fig. 4.5 for large magnetic fields [28].

[1] That means our numerically computed values of the sum of all the cross sections deviates by only about 1% of the constant given by the sum rule.

5 Summary and Future Prospects

We have considered an electron confined in an anisotropic quantum dot under the influence of an externally applied perpendicular magnetic field and in the presence of the spin-orbit interaction. For numerical evaluation of the energy spectra and the optical absorption spectra of the QDs we have considered the InAs quantum dot (because in such narrow-gap semiconductor system, the dominant source of the SO interaction is the structural inversion asymmetry, which leads to the Rashba SO interaction). The parameters of that system are already available in Sect. 2.3. We have indicated that the anisotropy of a QD alone causes lifting of degeneracies of the Fock-Darwin (i.e. single-electron) levels at $B = 0,$ as reported earlier [12]. However, when we also introduce the SO coupling, its primary effect is the rearrangement of some of the energy levels at small magnetic fields and level repulsions at high fields, which are magnified rather significantly as one introduces anisotropy in the quantum dot. These effects are explained as due to mixing of different spinor states for increasing strength of the SO coupling. As a consequence, the corresponding absorption spectra reveals anticrossing structures in the two main lines of the spectra as well as new, low-intense modes that appear with the main absorption lines. These additional features arise entirely due to the SOI and are a consequence of level crossings and level repulsions in the energy spectra. This prominent effects of the Rashba SOI predicted here could be confirmed experimentally in optical spectroscopy [1, 2, 25] and in experimental observation of the Fock-Darwin spectra of few-electron QDs [2, 29]. The optical absorption spectra investigated here are entirely different from the ones observed so far in isotropic QDs. In the present case, the spectra for different values of α strongly depend on the polarization of the incident light. Unlike in the isotropic case the transitions are from the states related to oscillations in the direction of the polarization. As the far-infrared absorption spectrum is very

well established in the case of isotropic QDs, we expect that the novel features of anisotropic QDs predicted here will be experimentally observed in the near future. Experimental observation of these optical modes that appear solely due to the presence of the SO coupling would be very exciting because that would be a major step forward in our quest to manipulate the spin dynamics in nanostructured systems via the SO coupling, which is the driving mechanism for the rapidly emerging field of semiconductor spintronics. The spin degree of freedom is known to be more beneficial in this respect than the electron charge, because spin is not coupled to the electromagnetic noise (unlike the charge) and therefore has a much longer coherence time [30]. This will facilitate the use of spin dynamics in the QDs for future electronic and information processing, in particular, in quantum computing and quantum communication [31]. Finally, it should be pointed out that coherent manipulation of electron spin via optical excitation in semiconductor QDs has already been reported in the literatures [32-34].

Figure 5.1. Energy spectrum (left panel) and dipole-allowed transition energies (right pannel) versus the magnetic field B (in Tesla) for four interacting electrons in InAs QD with $\alpha = 20$ meV nm [10]

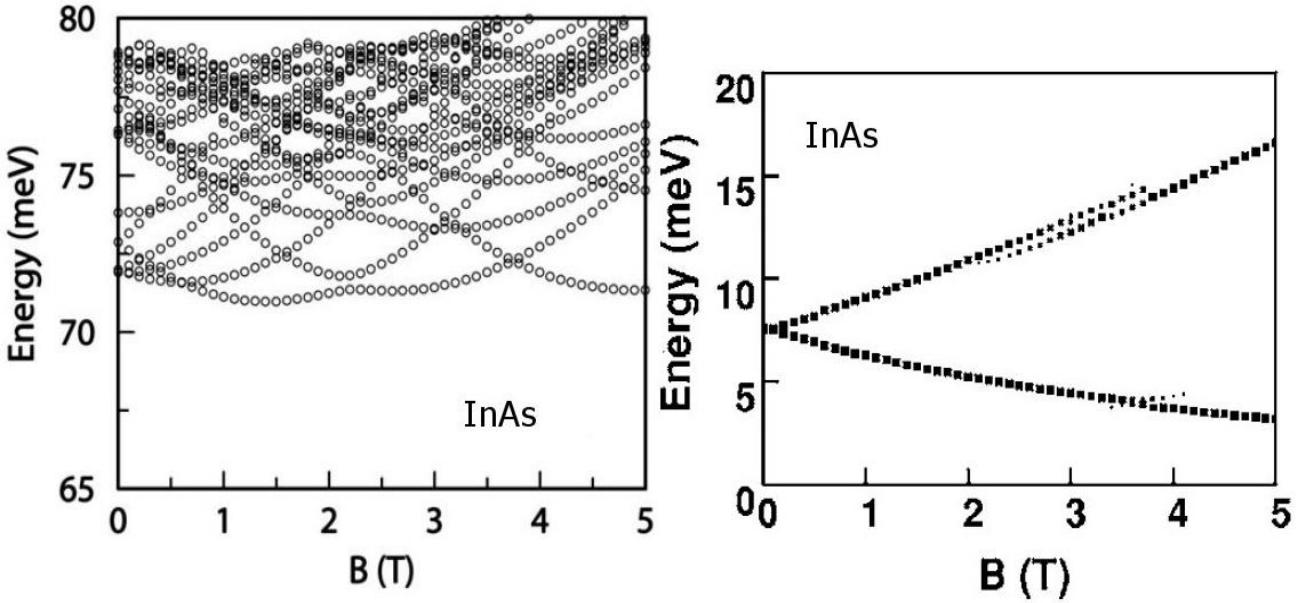

As it has been mentioned above, our studies reported here deal with the single-electron system. However, electron correlations in many-electron QDs have profound effects on the energy spectra. For isotropic QDs, the role of Coulomb interactions, in the presence of the Rashba SOI was explored by Chakraborty et al. [10]. For the interacting many-electron dots, one observes the appearance of additional anticrossings in the energy spectra and additional modes in the optical absorption spectra. In Fig. 5.1, we show the energy spectrum and optical absorption of a InAs isotropic QD containing four interacting electrons. The energy spectrum is clearly dense and requires quite extensive numerical computations. Similar studies of anisotropic QDs are very complex and will be the subject of our future work.

6 Appendices

Appendix A

Diaganalization of the Hamiltonian

A.1 The Rotated operators and the rotations

We define new operators

$$\begin{aligned} x &= q_1 \cos\chi - \chi_2 p_2 \sin\chi \\ y &= q_2 \cos\chi - \chi_2 p_1 \sin\chi \\ p_x &= p_1 \cos\chi + \chi_1 q_2 \sin\chi \\ p_y &= p_2 \cos\chi + \chi_1 q_1 \sin\chi. \end{aligned} \tag{A.1}$$

We also expand the Hamiltonian (2.1)

$$\begin{aligned} H &= \frac{1}{2m^*}\left[\mathbf{p} - \frac{e}{c}\mathbf{A}\right]^2 + V_{\text{conf}}(x,y) \\ &= \frac{1}{2m^*}\left[\left(p_x - \frac{e}{c}A_x\right)^2 + \left(p_y - \frac{e}{c}A_y\right)^2\right] + \frac{1}{2}m^*\left(\omega_x^2 x^2 + \omega_y^2 y^2\right) \\ &= \frac{1}{2m^*}\left[\left(p_x + \frac{eB}{2c}y\right)^2 + \left(p_y - \frac{eB}{2c}x\right)^2\right] + \frac{1}{2}m^*\left(\omega_x^2 x^2 + \omega_y^2 y^2\right) \\ &= \frac{1}{2m^*}\left[p_x^2 + \left(\frac{eB}{2c}\right)^2 y^2 + \frac{eB}{c}p_x y + p_y^2 + \left(\frac{eB}{2c}\right)^2 x^2 - \frac{eB}{c}p_y x\right] + \frac{1}{2}m^*\left(\omega_x^2 x^2 + \omega_y^2 y^2\right). \end{aligned} \tag{A.2}$$

Defining

$$\omega_c = \frac{eB}{m^* c}, \qquad \Omega_{1,2}^2 = m^{*2}\left(\omega_{x,y}^2 + \frac{1}{4}\omega_c^2\right)$$

the Hamiltonian (A.2) takes the form

$$
\begin{aligned}
H &= \frac{1}{2m^*}\left[\left(p_x^2 + p_y^2 \right) + \left(\frac{eB}{2c} \right)\left(x^2 + y^2 \right) + \frac{eB}{c}\left(yp_x - xp_y \right) \right] + \frac{1}{2} m^* \left(\omega_x^2 x^2 + \omega_y^2 y^2 \right) \\
&= \frac{1}{2m^*}\left(p_x^2 + p_y^2 \right) + \frac{1}{2} m^* \left(\omega_x^2 + \frac{1}{4}\omega_c^2 \right) x^2 + \frac{1}{2} m^* \left(\omega_y^2 + \frac{1}{4}\omega_c^2 \right) y^2 + \frac{1}{2}\omega_c \left(yp_x - xp_y \right) \\
&= \frac{1}{2m^*}\left(p_x^2 + p_y^2 \right) + \Omega_1^2 x^2 + \Omega_2^2 y^2 + m^* \omega_c \left(yp_x - xp_y \right).
\end{aligned}
\tag{A.3}
$$

Now let us look at the squares of the momentum operators:

$$
\begin{aligned}
p_x^2 &= \left(p_1 \cos\chi + \chi_1 q_2 \sin\chi \right)^2 \\
&= p_1^2 \cos^2\chi + \chi_1^2 q_2^2 \sin^2\chi + \chi_1 p_1 q_2 \cos\chi \sin\chi + \chi_1 q_2 p_1 \cos\chi \sin\chi \\
&= p_1^2 \cos^2\chi + \chi_1^2 q_2^2 \sin^2\chi + 2\chi_1 q_2 p_1 \cos\chi \sin\chi \\
&= p_1^2 \cos^2\chi + \chi_1^2 q_2^2 \sin^2\chi + \chi_1 q_2 p_1 \sin 2\chi
\end{aligned}
\tag{A.4}
$$

$$
\begin{aligned}
p_y^2 &= \left(p_2 \cos\chi + \chi_1 q_1 \sin\chi \right)^2 \\
&= p_2^2 \cos^2\chi + \chi_1^2 q_2^2 \sin^2\chi + 2\chi_1 q_1 p_2 \cos\chi \sin\chi \\
&= p_2^2 \cos^2\chi + \chi_1^2 q_1^2 \sin^2\chi + \chi_1 q_1 p_2 \sin 2\chi
\end{aligned}
\tag{A.5}
$$

where we have used the fundamental commutation relations (2.20). Next we transform the squares of the position operators:

$$
\begin{aligned}
x^2 &= \left(q_1 \cos\chi - \chi_2 p_2 \sin\chi \right)^2 \\
&= q_1^2 \cos^2\chi + \chi_2^2 p_2^2 \sin^2\chi - 2\chi_2 q_1 p_2 \cos\chi \sin\chi \\
&= q_1^2 \cos^2\chi + \chi_2^2 p_2^2 \sin^2\chi - \chi_2 q_1 p_2 \sin 2\chi
\end{aligned}
\tag{A.6}
$$

$$
\begin{aligned}
y^2 &= \left(q_2 \cos\chi - \chi_2 p_1 \sin\chi \right)^2 \\
&= q_2^2 \cos^2\chi + \chi_2^2 p_1^2 \sin^2\chi - 2\chi_2 q_2 p_1 \cos\chi \sin\chi \\
&= q_2^2 \cos^2\chi + \chi_2^2 p_1^2 \sin^2\chi - \chi_2 q_2 p_1 \sin 2\chi.
\end{aligned}
\tag{A.7}
$$

Finally, the cross terms are transformed:

$$
\begin{aligned}
xp_y &= \left(q_1 \cos\chi - \chi_2 p_2 \sin\chi \right)\left(p_2 \cos\chi + \chi_1 q_1 \sin\chi \right) \\
&= \chi_1 q_1^2 \cos\chi \sin\chi - \chi_2 p_2^2 \cos\chi \sin\chi + q_1 p_2 \cos^2\chi - \chi_1 \chi_2 q_1 p_2 \sin^2\chi \\
&= \chi_1 q_1^2 \cos\chi \sin\chi - \chi_2 p_2^2 \cos\chi \sin\chi + q_1 p_2 \cos 2\chi
\end{aligned}
\tag{A.8}
$$

$$
\begin{aligned}
yp_x &= \left(q_2\cos\chi - \chi_2 p_1 \sin\chi\right)\left(p_1\cos\chi + \chi_1 q_2 \sin\chi\right) \\
&= \chi_1 q_2^2 \cos\chi\sin\chi - \chi_2 p_1^2 \cos\chi\sin\chi + q_2 p_1 \cos^2\chi - \chi_1\chi_2 q_2 p_1 \sin^2\chi \\
&= \chi_1 q_2^2 \cos\chi\sin\chi - \chi_2 p_1^2 \cos\chi\sin\chi + q_2 p_1 \cos 2\chi
\end{aligned}
\tag{A.9}
$$

where we have applied the condition $\chi_1\chi_2 = 1$. In the Hamiltonian we need the combinations

$$
\begin{aligned}
p_x^2 + p_y^2 &= p_1^2\cos^2\chi + \chi_1^2 q_2^2 \sin^2\chi + \chi_1 q_2 p_1 \sin 2\chi \\
&\quad + p_2^2\cos^2\chi + \chi_1^2 q_1^2 \sin^2\chi + \chi_1 q_1 p_2 \sin 2\chi \\
&= \left(p_1^2 + p_2^2\right)\cos^2\chi + \chi_1^2\left(q_1^2 + q_2^2\right)\sin^2\chi + \chi_1\left(q_2 p_1 + q_1 p_2\right)\sin 2\chi
\end{aligned}
\tag{A.10}
$$

$$
\begin{aligned}
yp_x - xp_y &= \chi_1 q_2^2 \cos\chi\sin\chi - \chi_2 p_1^2 \cos\chi\sin\chi + q_2 p_1 \cos 2\chi \\
&\quad - \left(\chi_1 q_1^2 \cos\chi\sin\chi - \chi_2 p_2^2 \cos\chi\sin\chi + q_1 p_2 \cos 2\chi\right) \\
&= \chi_1\left(q_2^2 - q_1^2\right)\cos\chi\sin\chi + \chi_2\left(p_2^2 - p_1^2\right)\cos\chi\sin\chi + \left(q_2 p_1 - q_1 p_2\right)\cos 2\chi \\
&= \frac{1}{2}\chi_1\left(q_2^2 - q_1^2\right)\sin 2\chi + \frac{1}{2}\chi_2\left(p_2^2 - p_1^2\right)\sin 2\chi + \left(q_2 p_1 - q_1 p_2\right)\cos 2\chi.
\end{aligned}
\tag{A.11}
$$

The Hamiltonian then is

$$
\begin{aligned}
H = \Bigg\{ & \frac{1}{2m^*}\left(p_1^2 + p_2^2\right)\cos^2\chi + \chi_1^2\left(q_1^2 + q_2^2\right)\sin^2\chi + \chi_1\left(q_2 p_1 + q_1 p_2\right)\sin 2\chi \\
& + \left[\Omega_1^2 q_1^2\cos^2\chi + \Omega_1^2\chi_2^2 p_2^2 \sin^2\chi - \Omega_1^2\chi_2 q_1 p_2 \sin 2\chi\right] \\
& + \left[\Omega_2^2 q_2^2\cos^2\chi + \Omega_2^2\chi_2^2 p_1^2 \sin^2\chi - \Omega_2^2\chi_2 q_2 p_1 \sin 2\chi\right] \\
& + m^*\omega_c\left[\left(q_2 p_1 - q_1 p_2\right)\cos 2\chi + \frac{1}{2}\chi_1\left(q_2^2 - q_1^2\right)\sin 2\chi + \frac{1}{2}\chi_2\left(p_2^2 - p_1^2\right)\sin 2\chi\right]\Bigg\}
\end{aligned}
\tag{A.12}
$$

$$
\begin{aligned}
H = \frac{1}{2m^*}\Big\{ & p_1^2\left(\cos^2\chi+\Omega_2^2\chi_2^2\sin^2\chi-\frac{1}{2}\chi_2 m^*\omega_c\sin 2\chi\right)\\
& + p_2^2\left(\cos^2\chi+\Omega_1^2\chi_2^2\sin^2\chi+\frac{1}{2}\chi_2 m^*\omega_c\sin 2\chi\right)\\
& + q_1^2\left(\chi_1^2\sin^2\chi+\Omega_1^2\cos^2\chi-\frac{1}{2}\chi_1 m^*\omega_c\sin 2\chi\right)\\
& + q_2^2\left(\chi_1^2\sin^2\chi+\Omega_2^2\cos^2\chi+\frac{1}{2}\chi_1 m^*\omega_c\sin 2\chi\right)\\
& + q_2 p_1\left(\chi_1\sin 2\chi-\Omega_2^2\chi_2\sin 2\chi+m^*\omega_c\cos 2\chi\right)\\
& + q_1 p_2\left(\chi_1\sin 2\chi-\Omega_1^2\chi_2\sin 2\chi-m^*\omega_c\cos 2\chi\right)\Big\}.
\end{aligned}
\tag{A.13}
$$

Our aim is to get rid of the cross terms $q_i p_j$. For that purpose, by setting

$$
\chi_1\sin 2\chi-\Omega_2^2\chi_2\sin 2\chi+m^*\omega_c\cos 2\chi=0 \tag{A.14.1}
$$

or

$$
\chi_1\sin 2\chi-\Omega_1^2\chi_2\sin 2\chi-m^*\omega_c\cos 2\chi=0\,, \tag{A.14.2}
$$

we get the relation

$$
\tan 2\chi=\frac{m^*\omega_c}{\chi_1-\chi_2\Omega_1^2}=\frac{m^*\omega_c}{\chi_1-\chi_2\Omega_2^2}\,. \tag{A.15}
$$

It is clear that in the case $\Omega_1^2=\Omega_2^2$ we must either have $\omega_c=0$ or $\chi_1-\chi_2\Omega_1^2=\chi_1-\chi_2\Omega_2^2$.

Correspondingly the angle χ will be either 0 or $\pm\pi/4$.

Assuming now that $\Omega_1^2\neq\Omega_2^2$ we get the condition

$$
\chi_1-\chi_2\Omega_1^2=\chi_2\Omega_2^2-\chi_1 \qquad \text{or} \qquad 2\chi_1=\chi_2\left(\Omega_1^2+\Omega_2^2\right) \tag{A.16}
$$

Multiplying this by χ_1 and applying again the condition $\chi_1\chi_2=1$ we get

$$
2\chi_1^2=\chi_1\chi_2\left(\Omega_1^2+\Omega_2^2\right)=\left(\Omega_1^2+\Omega_2^2\right) \tag{A.17}
$$

and consequently

$$\chi_1 = \pm\left[\frac{1}{2}\left(\Omega_1^2+\Omega_2^2\right)\right]^{1/2}. \tag{A.17.1}$$

For the angle χ we have the equation

$$\begin{aligned}\tan 2\chi &= \frac{m^*\omega_c}{\chi_1-\chi_2\Omega_1^2} = m^*\omega_c\,\frac{\chi_1}{\chi_1^2-\chi_1\chi_2\Omega_1^2} = \pm\, m^*\omega_c\,\frac{\left[\frac{1}{2}\left(\Omega_1^2+\Omega_2^2\right)\right]^{1/2}}{\frac{1}{2}\left(\Omega_1^2+\Omega_2^2\right)-\Omega_1^2} \\ &= \mp\, m^*\omega_c\,\frac{\left[2\left(\Omega_1^2+\Omega_2^2\right)\right]^{1/2}}{\Omega_1^2-\Omega_2^2}.\end{aligned} \tag{A.18}$$

This equation remains valid for the special case $\Omega_1^2 = \Omega_2^2$, where we get $\chi = \mp\,\pi/4$.

So the remaining nonvanishing terms in the Hamiltonian (A.13) are

$$\begin{aligned}H &= \frac{1}{2m^*}\Big\{ p_1^2\left(\cos^2\chi+\Omega_2^2\chi_2^2\sin^2\chi-\frac{1}{2}\chi_2 m^*\omega_c\sin 2\chi\right) \\ &\quad + p_2^2\left(\cos^2\chi+\Omega_1^2\chi_2^2\sin^2\chi+\frac{1}{2}\chi_2 m^*\omega_c\sin 2\chi\right) \\ &\quad + q_1^2\left(\chi_1^2\sin^2\chi+\Omega_1^2\cos^2\chi-\frac{1}{2}\chi_1 m^*\omega_c\sin 2\chi\right) \\ &\quad + q_2^2\left(\chi_1^2\sin^2\chi+\Omega_2^2\cos^2\chi+\frac{1}{2}\chi_1 m^*\omega_c\sin 2\chi\right)\Big\} \\ &= \frac{1}{2m^*}\left\{\beta_1^2 p_1^2+\beta_2^2 p_2^2+\gamma_1^2 q_1^2+\gamma_2^2 q_2^2\right\}\end{aligned} \tag{A.19}$$

where we have set

$$\begin{aligned}\beta_1^2 &= \cos^2\chi+\Omega_2^2\chi_2^2\sin^2\chi-\frac{1}{2}\chi_2 m^*\omega_c\sin 2\chi \\ \beta_2^2 &= \cos^2\chi+\Omega_1^2\chi_2^2\sin^2\chi+\frac{1}{2}\chi_2 m^*\omega_c\sin 2\chi \\ \gamma_1^2 &= \chi_1^2\sin^2\chi+\Omega_1^2\cos^2\chi-\frac{1}{2}\chi_1 m^*\omega_c\sin 2\chi \\ \gamma_2^2 &= \chi_1^2\sin^2\chi+\Omega_2^2\cos^2\chi+\frac{1}{2}\chi_1 m^*\omega_c\sin 2\chi\end{aligned} \tag{A.20}$$

To proceed, we need to determine the expressions for the trigonometric functions in the Hamiltonian (A.19). First, we can write

$$\begin{aligned}\sin 2\chi &= \frac{\tan 2\chi}{\sqrt{1+\tan^2 2\chi}} \\ \cos 2\chi &= \frac{1}{\sqrt{1+\tan^2 2\chi}}.\end{aligned} \tag{A.21}$$

The denominator can then be written explicitly as

$$\begin{aligned}\sqrt{1+\tan^2 2\chi} &= \left[1+m^{*2}\omega_c^2\,\frac{2(\Omega_1^2+\Omega_2^2)}{\Omega_1^2-\Omega_2^2}\right]^{1/2} \\ &= \frac{[(\Omega_1^2-\Omega_2^2)^2+2m^{*2}\omega_c^2(\Omega_1^2+\Omega_2^2)]^{1/2}}{\Omega_1^2-\Omega_2^2}\end{aligned} \tag{A.22}$$

Defining a new "angular velocity" Ω_3^2 as

$$\Omega_3^2 = \left[\left(\Omega_1^2-\Omega_2^2\right)^2+2m^{*2}\omega_c^2\left(\Omega_1^2+\Omega_2^2\right)\right]^{1/2} \tag{A.23}$$

we can then write

$$\sqrt{1+\tan^2 2\chi} = \frac{\Omega_3^2}{\Omega_1^2-\Omega_2^2} \tag{A.24}$$

and consequently

$$\begin{aligned}\sin 2\chi &= \mp m^*\omega_c\,\frac{\left[2\left(\Omega_1^2+\Omega_2^2\right)\right]^{1/2}}{\Omega_3^2} \\ \cos 2\chi &= \frac{\Omega_1^2-\Omega_2^2}{\Omega_3^2}\end{aligned} \tag{A.25}$$

The remaining trigonometric expressions are derived from

$$\cos 2\chi = 2\cos^2\chi - 1 = 1 - 2\sin^2\chi$$

yielding

$$\sin^2\chi = \frac{1}{2}\left(1-\cos 2\chi\right) = \frac{\Omega_3^2-\Omega_1^2+\Omega_2^2}{2\Omega_3^2}$$
$$\cos^2\chi = \frac{1}{2}\left(1+\cos 2\chi\right) = \frac{\Omega_3^2+\Omega_1^2-\Omega_2^2}{2\Omega_3^2}. \qquad \text{(A.26)}$$

We now start writing down the explicit expressions for the coefficients in the diagonal Hamiltonian (A.19). We begin with

$$\begin{aligned}
\beta_1^2 &= \cos^2\chi + \Omega_2^2\chi_2^2\sin^2\chi - \frac{1}{2}\chi_2 m^*\omega_c \sin 2\chi \\
&= \frac{\Omega_3^2+\Omega_1^2-\Omega_2^2}{2\Omega_3^2} + \frac{2}{\Omega_1^2+\Omega_2^2}\Omega_2^2\frac{\Omega_3^2-\Omega_1^2+\Omega_2^2}{2\Omega_3^2} \\
&\quad \mp\frac{1}{2}\left[\frac{2}{\Omega_1^2+\Omega_2^2}\right]^{1/2} m^*\omega_c\left(\mp m^*\omega_c\frac{[2(\Omega_1^2+\Omega_2^2)]^{1/2}}{\Omega_3^2}\right) \\
&= \frac{\Omega_3^2+\Omega_1^2-\Omega_2^2}{2\Omega_3^2} + \frac{2}{\Omega_1^2+\Omega_2^2}\Omega_2^2\frac{\Omega_3^2-\Omega_1^2+\Omega_2^2}{2\Omega_3^2} + m^{*2}\omega_c^2\frac{1}{\Omega_3^2} \\
&= \frac{1}{2\Omega_3^2\left(\Omega_1^2+\Omega_2^2\right)}\left[\left(\Omega_1^2+\Omega_2^2\right)\left(\Omega_3^2+\Omega_1^2-\Omega_2^2\right)+2\Omega_2^2\left(\Omega_3^2-\Omega_1^2+\Omega_2^2\right)+2m^{*2}\omega_c^2\left(\Omega_1^2+\Omega_2^2\right)\right]
\end{aligned}$$

$$\begin{aligned}
\beta_1^2 &= \frac{1}{2\Omega_3^2\left(\Omega_1^2+\Omega_2^2\right)}\left[\left(\Omega_1^2+\Omega_2^2\right)\left(\Omega_3^2+\Omega_1^2-\Omega_2^2\right)+2\Omega_2^2\left(\Omega_3^2-\Omega_1^2+\Omega_2^2\right)+\Omega_3^4-\left(\Omega_1^2-\Omega_2^2\right)^2\right] \\
&= \frac{1}{2\Omega_3^2\left(\Omega_1^2+\Omega_2^2\right)}\left[\Omega_3^2\left(\Omega_1^2+\Omega_2^2\right)+\left(\Omega_1^2+\Omega_2^2\right)\left(\Omega_1^2-\Omega_2^2\right)+2\Omega_2^2\Omega_3^2-2\Omega_2^2\left(\Omega_1^2-\Omega_2^2\right)\right. \\
&\qquad \left.+\Omega_3^4-\left(\Omega_1^2-\Omega_2^2\right)^2\right] \qquad \text{(A.27)} \\
&= \frac{1}{2\Omega_3^2\left(\Omega_1^2+\Omega_2^2\right)}\left[\Omega_3^2\left(\Omega_1^2+3\Omega_2^2+\Omega_3^2\right)+\left(\Omega_1^2-\Omega_2^2\right)\left(\Omega_1^2+\Omega_2^2-2\Omega_2^2-\Omega_1^2+\Omega_2^2\right)\right]
\end{aligned}$$

$$= \frac{\Omega_3^2\left(\Omega_1^2+3\Omega_2^2+\Omega_3^2\right)}{2\Omega_3^2\left(\Omega_1^2+\Omega_2^2\right)} = \frac{\Omega_1^2+3\Omega_2^2+\Omega_3^2}{2\left(\Omega_1^2+\Omega_2^2\right)}$$

Similarly,

$$\begin{aligned}\beta_2^2 &= \frac{3\Omega_1^2+\Omega_2^2-\Omega_3^2}{2\left(\Omega_1^2+\Omega_2^2\right)}\\ \gamma_1^2 &= \frac{1}{4}\left[3\Omega_1^2+\Omega_2^2+\Omega_3^2\right]\\ \gamma_2^2 &= \frac{1}{4}\left[\Omega_1^2+3\Omega_2^2-\Omega_3^2\right].\end{aligned} \tag{A.28}$$

Appendix B

B.1 The Ladder operators

The ladder operators are

$$\begin{aligned}a_i &= \sqrt{\frac{m_i\omega_i}{2\hbar}}\left(q_i+\frac{i}{m_i\omega_i}p_i\right) = \frac{1}{\sqrt{2\hbar}}\left(\kappa_i q_i+\frac{i}{\kappa_i}p_i\right)\\ a_i^\dagger &= \sqrt{\frac{m_i\omega_i}{2\hbar}}\left(q_i-\frac{i}{m_i\omega_i}p_i\right) = \frac{1}{\sqrt{2\hbar}}\left(\kappa_i q_i-\frac{i}{\kappa_i}p_i\right)\end{aligned} \tag{B.1}$$

with $\kappa_i^2 = m_i\omega_i = \frac{\gamma_i}{\beta_i}$.

Solving these definitions for the position and momentum operators yields

$$\begin{aligned}q_i &= \sqrt{\frac{\hbar}{2m_i\omega_i}}\left(\mathrm{a}_i+\mathrm{a}_i^\dagger\right) = \sqrt{\frac{\hbar}{2}}\,\frac{1}{\kappa_i}\left(\mathrm{a}_i+\mathrm{a}_i^\dagger\right)\\ p_i &= i\sqrt{\frac{\hbar m_i\omega_i}{2}}\left(\mathrm{a}_i^\dagger-\mathrm{a}_i\right) = i\sqrt{\frac{\hbar}{2}}\,\kappa_i\left(\mathrm{a}_i^\dagger-\mathrm{a}_i\right).\end{aligned} \tag{B.2}$$

Defining the number operator N as

$$N = a^\dagger a \tag{B.3}$$

we derive the commutation relations

$$\begin{aligned}\left[a, a^{\dagger}\right] &= 1 \\ \left[N, a^{\dagger}\right] &= a^{\dagger} \\ \left[N, a\right] &= -a\end{aligned} \tag{B.4}$$

and the properties

$$\begin{aligned}a\left|n\right\rangle &= \sqrt{n}\left|n-1\right\rangle \\ a^{\dagger}\left|n\right\rangle &= \sqrt{n+1}\left|n+1\right\rangle\end{aligned} \tag{B.5}$$

which explains why a_i and $a_i^{\dagger}$ are also called lowering and raising operators. Here the states $\left|n\right\rangle$ are the eigenstates of the number operator, i.e.

$$N\left|n\right\rangle = n\left|n\right\rangle, \quad n = 0,1,2,... \tag{B.6}$$

With all these relations, we can now derive the matrix elements of q_i and p_i as

$$\begin{aligned}\left\langle n_1', n_2'\right|q_1\left|n_1, n_2\right\rangle &= \sqrt{\frac{\hbar}{2}}\frac{1}{\kappa_1}\left\langle n_1', n_2'\right|a_1^{\dagger} + a_1\left|n_1, n_2\right\rangle \\ &= \sqrt{\frac{\hbar}{2}}\frac{1}{\kappa_1}\left(\sqrt{n_1+1}\delta_{n_1', n_1+1}\delta_{n_2', n_2} + \sqrt{n_1}\delta_{n_1', n_1-1}\delta_{n_2', n_2}\right) \\ \left\langle n_1', n_2'\right|q_2\left|n_1, n_2\right\rangle &= \sqrt{\frac{\hbar}{2}}\frac{1}{\kappa_2}\left\langle n_1', n_2'\right|a_2^{\dagger} + a_2\left|n_1, n_2\right\rangle \\ &= \sqrt{\frac{\hbar}{2}}\frac{1}{\kappa_2}\left(\sqrt{n_2+1}\delta_{n_1', n_1}\delta_{n_2', n_2+1} + \sqrt{n_2}\delta_{n_1', n_1}\delta_{n_2', n_2-1}\right)\end{aligned} \tag{B.7}$$

$$\begin{aligned}\left\langle n_1', n_2'\right|p_1\left|n_1, n_2\right\rangle &= i\sqrt{\frac{\hbar}{2}}\kappa_1\left\langle n_1', n_2'\right|a_1^{\dagger} - a_1\left|n_1, n_2\right\rangle \\ &= i\sqrt{\frac{\hbar}{2}}\kappa_1\left(\sqrt{n_1+1}\delta_{n_1', n_1+1}\delta_{n_2', n_2} - \sqrt{n_1}\delta_{n_1', n_1-1}\delta_{n_2', n_2}\right) \\ \left\langle n_1', n_2'\right|p_2\left|n_1, n_2\right\rangle &= i\sqrt{\frac{\hbar}{2}}\kappa_2\left\langle n_1', n_2'\right|a_2^{\dagger} - a_2\left|n_1, n_2\right\rangle \\ &= i\sqrt{\frac{\hbar}{2}}\kappa_2\left(\sqrt{n_2+1}\delta_{n_1', n_1}\delta_{n_2', n_2+1} - \sqrt{n_2}\delta_{n_1', n_1}\delta_{n_2', n_2-1}\right).\end{aligned}$$

We will use the shorthand notations

$$\begin{aligned}\langle\lambda'|q_i|\lambda\rangle &= \langle n_1', n_2'|q_i|n_1, n_2\rangle \\ \langle\lambda'|p_i|\lambda\rangle &= \langle n_1', n_2'|p_i|n_1, n_2\rangle\end{aligned} \tag{B.8}$$

and

$$\begin{aligned}\Gamma^i_{\lambda'\lambda} &= \sqrt{n_i+1}\,\delta_{n_i',n_i+1}\delta_{n_j',n_j} + \sqrt{n_i}\,\delta_{n_i',n_i-1}\delta_{n_j',n_j}, \qquad \text{with } \; j = i+1 \\ \Delta^i_{\lambda'\lambda} &= \sqrt{n_i+1}\,\delta_{n_i',n_i+1}\delta_{n_j',n_j} - \sqrt{n_i}\,\delta_{n_i',n_i-1}\delta_{n_j',n_j}\end{aligned} \tag{B.9}$$

so that we can now write

$$\begin{aligned}\langle\lambda'|q_i|\lambda\rangle &= \sqrt{\frac{\hbar}{2}}\frac{1}{\kappa_i}\Gamma^i_{\lambda'\lambda} \\ \langle\lambda'|p_i|\lambda\rangle &= \sqrt{\frac{\hbar}{2}}\,\kappa_i\,\Delta^i_{\lambda'\lambda}.\end{aligned} \tag{B.10}$$

We also let Γ^i and Δ^i stand for the appropriate combinations of the ladder operators

$$\begin{aligned}\Gamma^i &= a_i^\dagger + a_i \\ \Delta^i &= a_i^\dagger - a_i\end{aligned} \tag{B.11}$$

so that the position and momentum operators can be written

$$\begin{aligned}q_i &= \sqrt{\frac{\hbar}{2}}\frac{1}{\kappa_i}\Gamma^i \\ p_i &= i\sqrt{\frac{\hbar}{2}}\,\kappa_i\,\Delta^i.\end{aligned} \tag{B.12}$$

B.2 Matrix elements of the Rashba SO coupling

We now turn our attention to the Rashba SO coupling

$$H_{SO} = \frac{\alpha}{\hbar}\left[\boldsymbol{\sigma}\times\left(\mathbf{p}-\frac{e}{c}\mathbf{A}\right)\right]_z = \frac{\alpha}{\hbar}\left[\sigma_x\left(p_y-\frac{e}{c}A_y\right)-\sigma_y\left(p_x-\frac{e}{c}A_x\right)\right]. \tag{B.13}$$

Since for the vector potential we chose $\mathbf{A} = \frac{1}{2}B(-y,\,x,\,0)$, we can write

$$
\begin{aligned}
\frac{\hbar}{\alpha} H_{SO} &= \sigma_x \left(p_y - \frac{eB}{2c} x \right) - \sigma_y \left(p_x + \frac{eB}{2c} y \right) \\
&= \sigma_x \left(\cos\chi\, p_2 + \sin\chi \chi_1 q_1 - \frac{eB}{2c} \cos\chi\, q_1 + \frac{eB}{2c} \sin\chi \chi_2 p_2 \right) \\
&- \sigma_y \left(\cos\chi\, p_1 + \sin\chi \chi_1 q_2 + \frac{eB}{2c} \cos\chi\, q_2 - \frac{eB}{2c} \sin\chi \chi_2 p_1 \right) \\
&= \sigma_x \left(\sin\chi\, \chi_1 - \cos\chi\, \omega_0 \right) \mathrm{q}_1 \\
&- \sigma_y \left(\sin\chi\, \chi_1 + \cos\chi\, \omega_0 \right) \mathrm{q}_2 \\
&- \sigma_y \left(\cos\chi - \sin\chi\, \omega_0\, \chi_2 \right) \mathrm{p}_1 \\
&+ \sigma_x \left(\cos\chi + \sin\chi\, \omega_0\, \chi_2 \right) \mathrm{p}_2 \\
&= \sigma_x \left(\sin\chi\, \chi_1 \tau_1 - \cos\chi\, \omega_0 \tau_1 \right) \Gamma^1 \\
&- \sigma_y \left(\sin\chi\, \chi_1 \tau_2 + \cos\chi\, \omega_0\, \tau_2 \right) \Gamma^2 \\
&- i\sigma_y \left(\cos\chi\, v_1 - \sin\chi\, \omega_0 \chi_2\, v_1 \right) \Delta^1 \\
&- i\sigma_x \left(\cos\chi\, v_2 + \sin\chi\, \omega_0 \chi_2\, v_2 \right) \Delta^2,
\end{aligned}
\tag{B.14}
$$

where $\omega_0 = eB/2c,\ \tau_i = \sqrt{\frac{\hbar}{2}} \frac{1}{\kappa_i},\ v_i = \sqrt{\frac{\hbar}{2}} \kappa_i$.

Introducing the short hand notations

$$
\begin{aligned}
r_1 &= \sin\chi\, \chi_1 \tau_1 - \cos\chi\, \omega_0 \tau_1 \\
r_2 &= \sin\chi\, \chi_1 \tau_2 + \cos\chi\, \omega_0\, \tau_2 \\
s_1 &= \cos\chi\, v_1 - \sin\chi\, \omega_0 \chi_2\, v_1 \\
s_2 &= \cos\chi\, v_2 + \sin\chi\, \omega_0 \chi_2\, v_2
\end{aligned}
\tag{B.15}
$$

we have

$$
\begin{aligned}
\frac{\hbar}{\alpha} H_{SO} &= \sigma_x r_1 \Gamma^1 - \sigma_y r_2 \Gamma^2 - i\sigma_y s_1 \Delta^1 + i\sigma_x s_2 \Delta^2 \\
&= \begin{pmatrix} 0 & 1 \\ 1 & 0 \end{pmatrix} r_1 \Gamma^1 - \begin{pmatrix} 0 & -i \\ i & 0 \end{pmatrix} r_2 \Gamma^2 - i \begin{pmatrix} 0 & -i \\ i & 0 \end{pmatrix} s_1 \Delta^1 + i \begin{pmatrix} 0 & 1 \\ 1 & 0 \end{pmatrix} s_2 \Delta^2 \\
&= \begin{pmatrix} 0 & r_1 \Gamma^1 + i r_2 \Gamma^2 \\ r_1 \Gamma^1 - i r_2 \Gamma^2 & 0 \end{pmatrix} + \begin{pmatrix} 0 & -s_1 \Delta^1 + i s_2 \Delta^2 \\ s_1 \Delta^1 + i s_2 \Delta^2 & 0 \end{pmatrix}.
\end{aligned}
\tag{B.16}
$$

The matrix elements of the SO operator are then

$$\begin{aligned}
\left\langle \lambda';\uparrow \left| \frac{\hbar}{\alpha} H_{SO} \right| \lambda;\downarrow \right\rangle &= r_1 \Gamma^1_{\lambda'\lambda} - s_1 \Delta^1_{\lambda'\lambda} + i(r_2 \Gamma^2_{\lambda'\lambda} + s_2 \Delta^2_{\lambda'\lambda}) \\
\left\langle \lambda';\downarrow \left| \frac{\hbar}{\alpha} H_{SO} \right| \lambda;\uparrow \right\rangle &= r_1 \Gamma^1_{\lambda'\lambda} + s_1 \Delta^1_{\lambda'\lambda} + i(-r_2 \Gamma^2_{\lambda'\lambda} + s_2 \Delta^2_{\lambda'\lambda}) \\
\left\langle \lambda';\uparrow \left| \frac{\hbar}{\alpha} H_{SO} \right| \lambda;\uparrow \right\rangle &= \left\langle \lambda';\downarrow \left| \frac{\hbar}{\alpha} H_{SO} \right| \lambda;\downarrow \right\rangle = 0.
\end{aligned} \tag{B.17}$$

Now, it is easy to see that

$$\begin{aligned}
\left\langle \lambda;\uparrow \left| \frac{\hbar}{\alpha} H_{SO} \right| \lambda';\downarrow \right\rangle &= r_1 \Gamma^1_{\lambda\lambda'} - s_1 \Delta^1_{\lambda\lambda'} + i\left(r_2 \Gamma^2_{\lambda\lambda'} + s_2 \Delta^2_{\lambda\lambda'} \right) \\
&= r_1 \Gamma^1_{\lambda'\lambda} + s_1 \Delta^1_{\lambda'\lambda} + i\left(r_2 \Gamma^2_{\lambda'\lambda} - s_2 \Delta^2_{\lambda'\lambda} \right) \\
&= \left\langle \lambda';\downarrow \left| \frac{\hbar}{\alpha} H_{SO} \right| \lambda;\uparrow \right\rangle^*
\end{aligned} \tag{B.18.1}$$

$$\begin{aligned}
\left\langle \lambda;\downarrow \left| \frac{\hbar}{\alpha} H_{SO} \right| \lambda';\uparrow \right\rangle &= r_1 \Gamma^1_{\lambda\lambda'} + s_1 \Delta^1_{\lambda\lambda'} + i\left(-r_2 \Gamma^2_{\lambda\lambda'} + s_2 \Delta^2_{\lambda\lambda'} \right) \\
&= r_1 \Gamma^1_{\lambda'\lambda} - s_1 \Delta^1_{\lambda'\lambda} + i\left(-r_2 \Gamma^2_{\lambda'\lambda} - s_2 \Delta^2_{\lambda'\lambda} \right) \\
&= \left\langle \lambda';\uparrow \left| \frac{\hbar}{\alpha} H_{SO} \right| \lambda;\downarrow \right\rangle^*,
\end{aligned} \tag{B.18.2}$$

which clearly proves the Hermiticity of the SO matrix.

B.3 The dipole transition matrix elements and the selection rules

The conventional position operators x, y are written in terms of q_i and p_i as in (A.1). Since we already know the matrix elements of q_i and p_i, it becomes a straightforward job to work out the matrix elements of x and y.

We need to evaluate,

$$\begin{aligned}
\left\langle n_1', n_2' \left| x \right| n_1, n_2 \right\rangle &= \left\langle n_1', n_2' \left| q_1 \cos\chi - \chi_2 p_2 \sin\chi \right| n_1, n_2 \right\rangle \\
&= \left\langle n_1', n_2' \left| q_1 \cos\chi \right| n_1, n_2 \right\rangle - \chi_2 \left\langle n_1', n_2' \left| p_2 \sin\chi \right| n_1, n_2 \right\rangle
\end{aligned} \tag{B.19.1}$$

Now, using the expressions in (B.7) we find

$$\begin{aligned}\langle n_1', n_2' | x | n_1, n_2 \rangle &= \sqrt{\frac{\hbar}{2}} \frac{1}{\kappa_1} \cos\chi \left(\sqrt{n_1 + 1}\, \delta_{n_1', n_1+1} \delta_{n_2', n_2} + \sqrt{n_1}\, \delta_{n_1', n_1-1} \delta_{n_2', n_2} \right) \\ &\quad - i \sqrt{\frac{\hbar}{2}} \kappa_2 \chi_2 \sin\chi \left(\sqrt{n_2 + 1}\, \delta_{n_1', n_1} \delta_{n_2', n_2+1} - \sqrt{n_2}\, \delta_{n_1', n_1} \delta_{n_2', n_2-1} \right)\end{aligned} \tag{B.19.2}$$

Similarly,

$$\begin{aligned}\langle n_1', n_2' | y | n_1, n_2 \rangle &= \langle n_1', n_2' | q_2 \cos\chi - \chi_2 p_1 \sin\chi | n_1, n_2 \rangle \\ &= \langle n_1', n_2' | q_2 \cos\chi | n_1, n_2 \rangle - \chi_2 \langle n_1', n_2' | p_1 \sin\chi | n_1, n_2 \rangle \\ &= \sqrt{\frac{\hbar}{2}} \frac{1}{\kappa_2} \cos\chi \left(\sqrt{n_2 + 1}\, \delta_{n_1', n_1} \delta_{n_2', n_2+1} + \sqrt{n_2}\, \delta_{n_1', n_1} \delta_{n_2', n_2-1} \right) \\ &\quad - i \sqrt{\frac{\hbar}{2}} \kappa_1 \chi_2 \sin\chi \left(\sqrt{n_1 + 1}\, \delta_{n_1', n_1+1} \delta_{n_2', n_2} - \sqrt{n_1}\, \delta_{n_1', n_1-1} \delta_{n_2', n_2} \right)\end{aligned} \tag{B.20}$$

The selection rules for the transitions to higher energy levels are now obvious.

When we have polarization along the x axis they are as follows:

$$\begin{aligned}&(i) \quad \Delta n_1 = \pm 1, \qquad \Delta n_2 = 0 \\ &(ii) \quad \Delta n_1 = 0, \qquad \Delta n_2 = \pm 1,\end{aligned} \tag{B.21.1}$$

and for the polarization along the y axis:

$$\begin{aligned}&(i) \quad \Delta n_1 = 0, \qquad \Delta n_2 = \pm 1 \\ &(ii) \quad \Delta n_1 = \pm 1, \qquad \Delta n_2 = 0.\end{aligned} \tag{B.21.2}$$

Bibliography

[1] T. Chakraborty, *Quantum Dots* (North-Holland, Amsterdam, 1999); Comments Condens. Matter Phys. **16**, 35 (1992); P. A Maksym and T. Chakraboty, Phys. Rev.Lett. **65**, 108 (1990).

[2] *Quantum Materials*, edited by D. Heitmann (Springer, Heidelberg, 2010); Detlef Heitmann and Jorg P. Kotthaus, Physics Today, Vol. **46**, June 1993, p.56; Pierre M. Petroff, Axel Lorke, and Atac Imamoglu, Physics Today, Vol. **54,** (2001) p. 46.

[3] R.C. Ashoori, H.L. Störmer. J.S. Weiner, L.N. Pfeiffer, K.W. Baldwin, and K.W. West, Phys. Rev. Lett. **71**, 613 (1993).

[4] B. Meurer, D. Heitmann, and K. Ploog, Phys. Rev. Lett. **68,** 1371 (1992).

[5] R. Winkler, *Spin-orbit coupling effects in two-dimensional electron and hole system* (Springer, Heidelberg, 2003).

[6] Y. A. Bychkov and E. I. Rashba, J. Phys. C **17**, 6039 (1984).

[7] H. A. Engel, B. I. Halperin, and E. I. Rashba, Phys. Rev. Lett. **95**, 166605 (2005).

[8] G. Dresselhaus, Phys. Rev. **100**, 580 (1955).

[9] In InAs quantum well structures, the Dresselhaus SO interaction is quite appreciable, although the Rashba contribution is dominant; see, e.g., S. Giglberger *et al.*, Phys. Rev. B **75**, 035327 (2007).

[10] T. Chakraborty and P. Pietiläinen, Phys. Rev. Lett. **95**, 136603 (2005); P. Pietiläinen and T. Chakraborty, Phys. Rev. B **73**, 155315 (2006); T. Chakraborty and P. Pietiläinen, Phys. Rev. B **71**, 113305 (2005); and references therein.

[11] H. – Y. Chen, V. Apalkov, and T. Chakraborty, Phys Rev. B **75**, 193303 (2007).

[12] A. V. Madhav and T. Chakraborty, Phys. Rev. B **49**, 8163 (1994).

[13] A. Singha, V. Pellegrini, S. Kalliakos, B. Karmakar, A. Pinczuk, L. N. Pfeiffer, and K. W. West, Appl. Phys. Lett. **94**, 073114 (2009); D.G Austing, S. Sasaki, S. Tarucha, S. M. Reimann, M. Koskinen, and M. Manninen, Phys. Rev. B **60**, 11514 (1999); P.A. Maksym, Physica B **249-251,** 233 (1998); Y. Tokura, S. Sasaki, D.G. Austing, and S. Tarucha, Physica B **298,** 260 (2001).

[14] S. Avetisyan, P. Pietiläinen, and T. Chakrabrty, Phys. Rev. B **85**, 153301 (2012); **86**, 239901(E) (2012).

[15] For recent comprehensive reviews, see *Spintronics*, edited by T. Dietl, D. D. Awschalom, M. Kaminska, and H. Ono (Elsevier, Amsterdam, 2008); I. Zutic, J. Fabian, and S. Das Sarma, Rev. Mod. Phys. **76**, 323 (2004); J. Fabian, A. Matos-Abiague, C. Ertler, P. Santo, and I. Zutic, Acta Phys. Slov. **57**, 565 (2007); M. W. Wu, J. H. Jiang, and M. Q. Weng, Phys. Rep. **493**, 61 (2010).

[16] L. Landau, Z. Physik **64**, 629 (1930).

[17] R. Haupt and L. Wendler, Physica B **184**, 394 (1993).

[18] T. Chakraborty, V. Halonen, and P. Pietiläinen, Phys. Rev. B **43**, 14289 (1991).

[19] J. Nitta, T. Akazaki and H. Takayanagi, Phys. Rev. Lett. **28**, 1335 (1997);

[20] J. Nitta. T. Akazaki, H. Takayanagi and T. Enoki, Physica E **2**, 527 (1998).

[21] Y. Oreg, P. W. Brouner, X. Waintal, and B. I. Halperin, in *Nano-Physics Bio- Electronics: A New Odyssey*, edited by T. Chakraborty, F. Peeters, and U. Sivan (Elsevier, Amsterdam, 2002).

[22] J. Nitta, T. Akazaki, H. Takayanagi and T. Enoki, Phys. Rev. Lett. **78**, 1335 (1997); M. Studer, G. Salis, K. Ensselin, D. C. Driscoll, and A. C. Gossard, Phys. Rev. Lett. **103**, 027201 (2009); D. Grundler, Phys. Rev. Lett. **84**, 6074 (2000).

[23] H. Sanada, T. Sogawa, H. Gotoh, K. Onomitsu, M. Kohda, J. Nitta, and P. V. Santos, Phys. Rev. Lett. **106**, 216602 (2011); S. Takahashi, R. S. Deacon, K. Yoshida, A. Oiwa, K. Shibata, K. Hirakawa, Y. Tokura, and S. Tarucha, Phys. Rev. Lett. **104**, 246801 (2010).

[24] M. P. Nowak, B. Szafran, F. M. Peeters, B. Partoens, and W. J. Pasek, Phys. Rev. B **83**, 245324 (2011).

[25] Ch. Sikorski and U. Merkt, Phys. Rev. Lett. **62**, 2164 (1989).

[26] T. Demel, D. Heitmann, P.Grambow, and K. Ploog, Phys. Rev. Lett. **64**, 788 (1990).

[27] J. J. Sakurai and J. Napolitano, *Modern Quantum Mechanics*, 2nd ed. (Addison-Wesley, New York, 1994) p. 368; W. Thomas, Naturwissenschaften **13**, 627 (1925); W. Kuhn, Z. Phys. **33**, 408 (1925); F. Reiche and W. Thomas, Z. Phys. **34**, 510 (1925).

[28] The sum rule was discussed earlier in the context of few- electron QDs with Rashba SO coupling by P. Lucignano, B. Jouault, and A. Tagliacozzo, Phys. Rev. B **75**, 153310 (2007).

[29] L. P. Kouwenhoven, D. G. Austing, and S. Tarucha, Rep. Prog. Phys. **64**, 701 (2001); A. Babinski, M. Potemski, S. Raymond, J. Lapointe, and Z. R. Wasilewski, Phys. Status Solidi C **3**, 3748 (2006); V. Pellegrini and A. Pinczuk, Phys. Status Solidi B **243**, 3617 (2006).

[30] S. Bandyopadhyay, Phys. Rev. B **61**, 13813 (2000).

[31] M. A. Eriksson, M. Friesen, S. N. Coppersmith, R. Joynt, L. J. Klein, K. Slinker, C. Tahan, P.M. Mooney, J. O. Chu, and S. J. Koester, Quantum Inf. Process. **3**, 133 (2004); D. Loss, G. Burkard, and D. P. DiVincenzo, J. Nanopart. Res. 2, 401 (2000); R. Hanson, L. H. Willems van Beveren, I. T. Vink, J. M. Elzerman, W. J. M. Naber, F. H. L. Koppens, L. P. Kouwenhoven, and L. M. K. Vandersypen, Phys. Rev. Lett. **94**, 196802 (2005); D. Stepanenko and N. E. Bonesteel, Phys. Rev. Lett. **93**, 140501 (2004).

[32] S. Cortez, O. Krebs, S. Laurent, M. Senes, X. Marie, P. Voisin, R. Ferreira, G. Bastard, J. M. Gerard and T. Amand, Phys. Rev. Lett. **89**, 207401 (2002).

[33] T. Calarco, A. Datta, P. Fedichev, E. Pazy, and P. Zoller, Phys. Rev. A **68**, 012310 (2003), Ren-Bao Liu, Wang Yao and L. J. Sham, Advances in Physics **59**, 703 (2010).

[34] D. D. Awschalom, D. Loss, and N. Samarthe (Eds.) Semiconductor Spintronics and Quantum Computation (Springer, 2002)